AN ABSTRACT OF THE THESIS OF

STEVEN REID SMITH for the degree of DOCTOR OF PHILOSOPHY

in Chemistry presented on January 4, 1977

Title: GAS PHASE X-RAY PHOTOELECTRON SPECTROSCOPY OF COMPOUNDS CONTAINING MULTIPLY-BONDED OXYGEN

Abstract approved: T. Darrah Thomas

A new x-ray source capable of operating at up to 80 watts has been designed and developed, and put to use with the Oregon State University Cylindrical Electrostatic Analyzer. The new source produces over four times the photoelectron intensity of its predecessor, from gaseous samples, and accommodates a wider selection of anode materials. Modifications have been proposed to increase the x-ray intensity by an additional factor of two to three.

Carbon 1s and oxygen 1s ionization energies have been measured for 11 esters, 4 acids, acetone, and carbon monoxide. In addition, oxygen 1s ionization energies have been estimated on the basis of the measured chemical shifts of the corresponding ethyl esters for three halogen-substituted acids that could not be measured themselves. A procedure for computing the uncertainty of individual

ionization energy measurements has been formulated and employed, facilitating the computation of weighted mean values from repeated measurements and of the uncertainty of the mean values.

Some preliminary results from this study were employed to establish that the correlation of core ionization energies with proton affinities previously reported for singly-bonded oxygen also applies to compounds containing doubly-bonded oxygen. This correlation allowed the conclusion to be reached that the doubly-bonded oxygen provides the site of protonation for acids and esters in the gas phase. In the light of new gas-phase proton affinity measurements, the slope of the core ionization energy-proton affinity correlation has been shown to be about -1.6 rather than the previously observed -1. It was suggested that shifts due to inductive effects and relaxation effects might correlate with different slopes, but this could not be verified on the basis of the data.

The relationship of core ionization energies to gas phase acidities (anionic proton affinities) has been investigated. The two quantities correlate for the fluorine-substituted acetic acids with a slope of -1.1. Using this result and an assumption relating the relaxation shifts, an empirical method of separately evaluating inductive and relaxation shifts has been developed. The results from this approach are in good agreement with those from semi-

empirical potential model calculations and with chemical intuition.

Finally, a four-parameter equation that was developed to analyze and predict substituent effects on the energies of certain gas-phase ionization processes has been extended to apply to most of the compounds included in this study. The carbonyl carbon 1s and oxygen 1s ionization energies were predicted with an average deviation from experiment of about 0.1 eV and 0.2 eV, respectively. Substituent parameters for the hydroxyl and ethoxy groups were determined.

Gas Phase X-Ray Photoelectron Spectroscopy of Compounds Containing Multiply-Bonded Oxygen

by

Steven Reid Smith

A THESIS

submitted to

Oregon State University

in partial fulfillment of
the requirements for the
degree of

Doctor of Philosophy

June 1977

APPROVED:

Redacted for Privacy

Professor of Chemistry in charge of major

Redacted for Privacy

Head of Department of Chemistry

Redacted for Privacy

Dean of Graduate School

Date thesis is presented January 4, 1977

Typed by Deanna L. Cramer for Steven Reid Smith

ACKNOWLEDGEMENTS

I gratefully acknowledge the guidance and support of Professor T. Darrah Thomas. His knowledge and his attributes of helpfulness and patience make him an excellent teacher and research advisor. I have appreciated the Research Assistantship, supported by the U.S. Energy Research and Development Administration and also by the National Science Foundation, under which this work was accomplished.

I have enjoyed my association with all the members of Professor Thomas's research group. Those who have contributed significantly to this work through helpful conversations and through sharing with me their experiences with the new x-ray source are Dr. Thomas X. Carroll, Dr. James S. Jen, Dr. Seppo Aksela, Mr. Scott Chambers, Mr. Kenneth Bomben and Mr. Patrick Sitton.

I have appreciated the work of Mr. Robert Mang, Mr. Doyle Woodrow and Mr. Patrick Sitton in constructing the x-ray source. I am grateful to Mrs. Dana Cramer for typing the manuscript.

Finally, I am grateful to my parents, who instilled in me the desire to learn and to succeed, and to my wife, Janice, who has supported my efforts wholeheartedly.

TABLE OF CONTENTS

Table of Contents -- continued

LIST OF TABLES

LIST OF ILLUSTRATIONS

GAS PHASE X-RAY PHOTOELECTRON SPECTROSCOPY OF COMPOUNDS CONTAINING MULTIPLY-BONDED OXYGEN

PART ONE

X-RAY GENERATION

I. GENERAL INTRODUCTION

The development in the 1950's of high resolution analyzers for beta-ray spectroscopy [1] opened the way for the emergence of an important group of other experimental techniques that require high resolution of the energy (or momentum) of electrons [2-5]. One of these techniques is x-ray photoelectron spectroscopy (XPS). The irradiation of sample materials with x-rays of known energy $h\nu$ causes the ejection of photoelectrons whose ionization energies E_i contain much information about the sample. Ionization energies are obtained from measured photoelectron kinetic energies K by the simple conservation of energy equation[1]

$$E_i = h\nu - K \qquad \text{(Eq. 1.1)}$$

XPS research has focused primarily on the study of "core" electrons, i.e., electrons whose distribution and energy are not greatly affected by changes in the chemical

---

[1] For atoms and small molecules in the gas phase, a correction for the recoil energy of the ion may be necessary. For condensed-phase samples, the work functions of the spectrometer and sample enter into this expression.

environment of the atom. The core ionization energies of each element are unique, thus providing a straightforward approach for qualitative analysis of the sample material.[2] Chemical effects do, however, influence core ionization energies, and the resulting "chemical shifts" have proved to be of great interest. Much of the XPS research conducted in this laboratory has been directed toward the observation and interpretation of chemical shifts in small molecules in the gas phase [6-11]. The instrument designed and developed by Citrin, Shaw, and Thomas (Figure 1) [12], now known as the Oregon State University Cylindrical Electrostatic Analyzer, is generally well-suited for this work.

One of the first objectives of this research was to design and develop a new x-ray source, which would enhance the usefulness of the OSU instrument by increasing its productivity and its versatility. The attainment of this objective is discussed in Part One. Part Two presents the techniques and results of a gas-phase XPS study of a group of molecules that contain multiply-bonded oxygen. The observed oxygen 1s chemical shifts are correlated with gas-phase acidities and proton affinities. Initial-state effects (induction) and final-state effects (polarization) are distinguished.

---

[2]Hence the acronym ESCA -- Electron Spectroscopy for Chemical Analysis -- which is sometimes used interchangeably with XPS and sometimes used to include other aspects of electron spectroscopy as well.

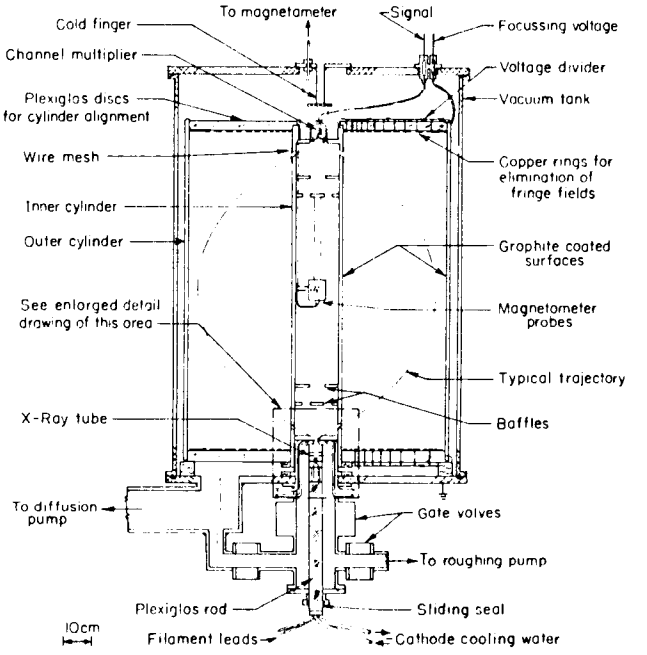

Figure 1. Oregon State University Cylindrical Electrostatic Analyzer in cross section. (From reference 12)

II. X-RAY GENERATION FOR XPS

The need for x-radiation of known energy is met in most XPS instruments by generating the characteristic x-rays of aluminum or magnesium. The $K\alpha_{1,2}$ doublet is unresolved in both cases, and is sufficiently narrow for most experimental requirements. The full width at half maximum is 0.81 eV [13] for Al $K\alpha_{1,2}$; it is somewhat less for Mg $K\alpha_{1,2}$ because both the spin-orbit splitting and the individual linewidths decrease with atomic number. The mean x-ray energies are 1486.582 ± .019 eV [14] and 1253.619 ± .026 eV [15, 16], respectively. Electron bombardment of the target metal in an evacuated chamber is the common method of x-ray production.

The accelerating voltage of the electron beam must be above the threshold for ionization of the state that will lead to the desired x-ray. For example, the Al $K\alpha_{1,2}$ threshold voltage is equal to the aluminum 1s ionization potential, 1558 V [17]. Increasing the accelerating voltage V beyond the threshold value V_o causes increased probability of core ionization, and results in greater characteristic x-ray intensity. The empirical intensity-voltage relationship for thick, solid targets [18] may be expressed in the form

$$N = k[(V-V_o)/V_o]^n \qquad \text{(Eq. 2.1)}$$

where N is the number of Kα quanta generated per steradian per incident electron. The constants k and n have been evaluated for Al $K\alpha_{1,2}$ [18] as 1.4×10^{-5} and 1.63, respectively, and include corrections to account for the x-rays absorbed within the target. The relation is accurate up to $V = 10\ V_o$, or 15 kV for Al $K\alpha_{1,2}$.

Two fundamental x-ray source design problems are evident in the above equation. First, the small value of k indicates that characteristic x-ray production by electron bombardment is very inefficient. At an accelerating voltage of 10 kV, the energy appearing as Al $K\alpha_{1,2}$ radiation accounts for only .03 percent of the electron beam energy incident at the anode. Even after subtracting the continuous x-ray energy component, about 99.9 percent of the incident energy is left as heat to be dissipated from the anode. Thus, an upper limit on the power used for electron bombardment is defined by, and essentially equal to, the rate at which heat can be removed from the anode at a temperature safely below its melting point.

The efficiency of characteristic x-ray generation is given by N/V, the number of Kα quanta generated per unit electron beam energy. This is an increasing function of the accelerating voltage, but is independent of the anode current. Accordingly, the maximum voltage difference that can be maintained between the filament and the anode sets an upper limit on the efficiency of x-ray production.

Electrode and insulator geometry and surface condition influence the discharge voltage, as do the nature and pressure of residual gas.

The heat-removal or power limit and the high-voltage limit are critical parameters of x-ray source performance. Another phenomenon that may restrict performance is surface sputtering of the anode. This may occur at a bulk temperature well below the melting point if the electron beam is focussed on a small area [19]. The power limitation caused by sputtering can be avoided by increasing the area of the focal spot or rotating the anode.

Another restriction on x-ray source performance arises because tungsten evaporates or is chemically abstracted from the hot filament and gradually coats the anode. This continually growing surface layer reduces the desired x-ray intensity by interacting with both incident electrons and out-going x-rays. Eventually the effect is sufficient to require cleaning and repolishing of the anode surface. The rate of tungsten deposition depends on electrode geometry and filament temperature.

Initial X-Ray Source of the OSU Instrument

The x-ray source designed and developed by Citrin, Shaw and Thomas [12] employs a thin foil anode which serves simultaneously as the window. This transmission-target design allows efficient use of the x-rays produced.

However, it is inherently limited in power (and thus intensity) by poor heat dissipation in the foil. The operational lifetime of 6.4 μm aluminum foil anode-windows decreases from days to hours when the power delivered to the anode is raised from 15 to 20 watts. Magnesium foil lifetimes of hours are attainable only below 10 watts.

This intensity restriction became more significant as interest developed in studying the vapor of less volatile liquids and in observing less intense photoelectron peaks and shake-up satellites. The use of anode materials not well suited for the thin foil anode window system was also desirable. These trends in research interest led to the decision to design and construct a new x-ray source, which would produce greater intensity and also allow the use of a wider variety of anode materials.

III. DESIGN AND DEVELOPMENT OF A NEW X-RAY SOURCE

To make effective use of the existing spectrometer structure, with its cylindrical mirror electrostatic analyzer, and to minimize cost, several constraints were imposed on the new design. These included cylindrical symmetry about the analyzer axis, adaptability to the existing sample cell for both gaseous and solid samples, and adaptability to the existing cooling system and electrical connections.

Several objectives were considered in working out a design enabling higher performance within the above constraints. The parameters to be maximized were: heat conductivity between the x-ray generation site and the water-cooled base, high voltage capacity, surface area of the x-ray generation site, and anode interchangeability. Those to be minimized were: rate of tungsten deposition on the anode and distance from the x-ray generation site to the window. These objectives are interrelated and somewhat mutually exclusive, necessitating compromises among them in the design.

The basic ideas for the new design arose from consideration of the objectives and constraints discussed above. A simple test-model x-ray source was constructed, and operated in a bell jar. A proportional counter served as the detector. On the basis of this experience, an

operational model was then built, and tested in the spectrometer. After several cycles of testing and modifying, the new source came into regular use for XPS experiments. Later modifications resulted in further increases in performance. Figure 2 shows the final design in cross section.

The anode is a single piece of target material, consisting of a large diameter base, a stem, and an approximately hemisperhical tip. The bottom of the anode base and the surface beneath it are polished to maximize thermal and electrical conductivity across the junction. The top half of the anode and the surfaces near it are also polished: surface roughness in these areas promotes high voltage discharge. The hemispherical tip serves as the x-ray generation site. Most of the surface area of the tip that is seen from the window is actually used for x-ray generation. The pattern made by tungsten deposition on the anode (see A, below) bears this out, as does the pattern of sputtered anode material after the power limit has been exceeded.

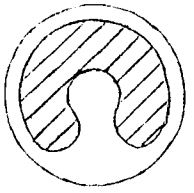

Scale 3:1

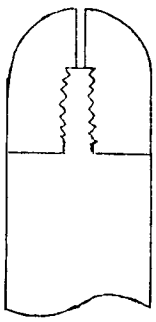

Top view,
One-piece anode

A

Cross section,
Two-piece anode

B

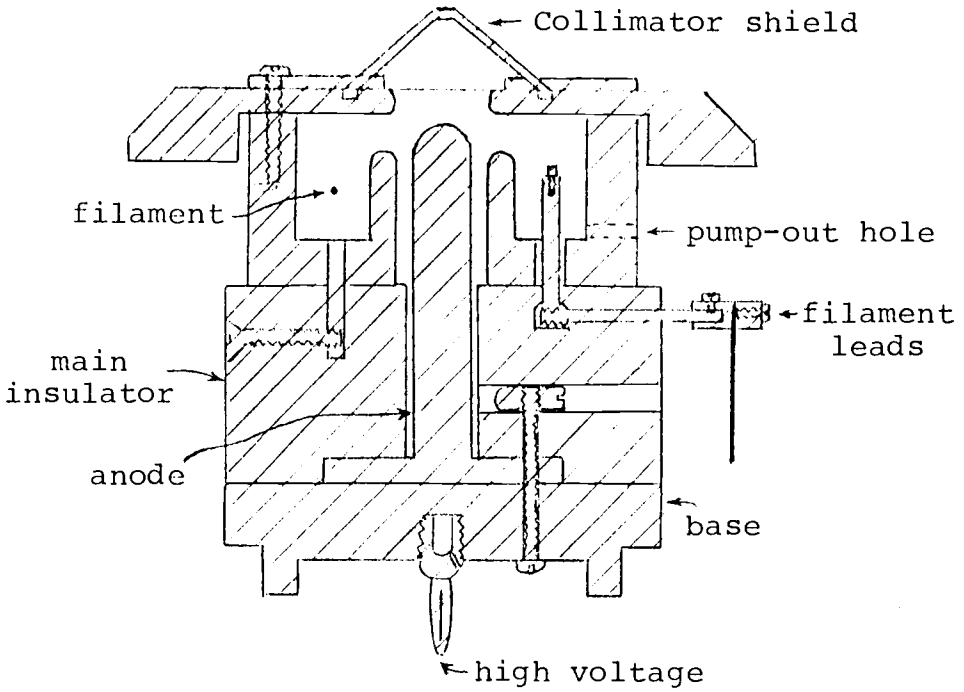

Cross-sectional view

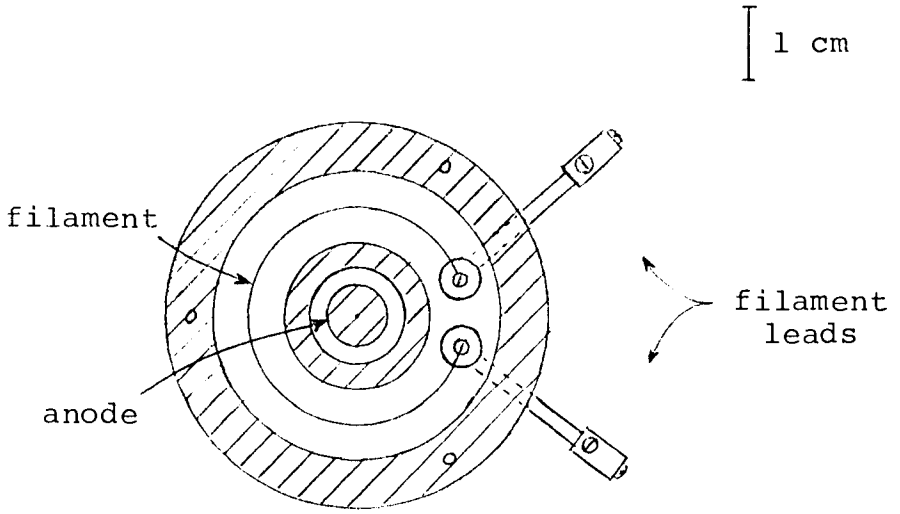

Top view of filament chamber

Figure 2. New x-ray source design.

An alternative anode design (see B, above) differs in that the base and stem are made of copper, while a detachable tip, about 6 mm in length, is made of the target material. The tip screws onto a threaded extension of the copper stem and has a tiny pump-out hole to prevent the trapping of air around the threads. The diameter of the stem is 5.6 mm, compared to 7.9 mm for the one-piece anode described above.

The grounded cylinder between the anode and filament has two main purposes. It shapes the electric field so as to focus the accelerating electrons on the useful x-ray generation site, and it blocks the line of sight between the filament and anode, thus reducing the rate of tungsten deposition.

The filament is an 8 cm length of 1 percent thoriated tungsten wire, 0.25 mm in diameter. It is supported at each end by a brass rod and held tightly in place by a set-screw. The base of each rod is mounted in the main insulator. Glass tubes insulate the rods and hold them in position at the openings into the filament chamber. A lead for outside electrical connections to the filament screws into the base of each supporting rod. Outside connections proved to be necessary to avoid high voltage discharges.

The filament chamber and lid are made of copper. Its high thermal conductivity promotes the flow (to a cooling

coil) of heat radiated by the filament. This part of the x-ray source is electrically grounded, with its upper surface serving as the bottom of the sample chamber.

The 6.4 μm-thick aluminum foil window is held in place by either of two aluminum rings. One of the rings also holds the collimator shield (see Figure 2); which reduces the carbon and oxygen background peaks by preventing irradiation of the collimator.

Lava, an unbaked ceramic material, was used for the main insulator. Lava is easily machinable, but does not hold screw threads well. The design thus relies on a less-direct method of holding the x-ray source firmly together.

The base of the new source attaches to a pre-existing receptacle, which contains the main cooling coil and the high-voltage connections. The base is made of copper, since its purpose is to provide effective thermal and electrical transmission between the anode and the receptacle.

IV. PRESENT PERFORMANCE AND FUTURE DEVELOPMENT OF THE X-RAY SOURCE

Counting Rate

The most pertinent test of the new x-ray source is how it performs in contrast with the old source. Specifically, how much greater is the photoelectron or Auger electron counting rate due to the new source, when identical spectra are recorded with each source operating at its optimum level.[3] Recent gas-phase experiments by T. D. Thomas and K. Bomben indicate that the counting rate is greater by a factor of 4.3 with the new x-ray source. This improvement allows a decrease of similar magnitude in the duration of gas-phase experiments. Thus, more measurements can be made in a given period of time, and each spectrum is less likely to be distorted by fluctuation of the focusing voltage or sample pressure. For gas phase work, the new source constitutes a significant improvement, and its creation is justified.

The optimum levels are about 15 watts at 10 kV for the old source and 80 watts at 10 kV for the new source. The new source requires 5.4 times as much power to generate 4.3 times as much electron intensity. It is thus 20

---

[3] "Optimum level" here refers to the highest combination of voltage and power that can be employed safely for experiments of several hours' duration.

percent less efficient in terms of counting rate per unit power. This is understandable, since, by virtue of the difference in anode-window designs, a smaller percentage of the x-rays produced by the new source actually reach the sample chamber.

The inherent advantage (in efficiency) of the transmission-target design over the new design is greatly multiplied in the case of solid samples. As a result, the old source produces greater counting rates from solid samples despite its lower optimum power level. Observations by Thomas and Bomben of the gold 4f photoelectron spectrum indicate that the counting rate advantage of the old source is a factor of 2.3 for a "ring-" or "sleeve"-mounted [20] gold foil sample and about a factor of ten for gold evaporated onto the surface of the window. Thus, using the new x-ray source to study solids is justified only if an anode material other than aluminum is required.

Accelerating Voltage

As was indicated in Chapter II, the voltage used to accelerate electrons from the filament to the anode is an important parameter of x-ray intensity. The empirical relationship of x-ray intensity to accelerating voltage cited previously,

$$N = k[(V-V_o)/V_o]^n \qquad \text{(Eq. 2.1)}$$

also fits data for the neon 1s photoelectron counting rate as a function of voltage. The proportionality constant k is arbitrary, of course. Four sets of data, obtained using an aluminum anode in the new x-ray source, fit the function with exponents n ranging from 1.65 to 1.90 and averaging 1.80. This is in approximate agreement with the value of 1.63 reported by Green and Cosslett [18] for the Al $K\alpha_{1,2}$ x-rays. The photoelectron counting rate thus increases with accelerating voltage at least as fast as was anticipated.

The new x-ray source can usually be operated with an accelerating voltage of 10 kV. However, there are two problems, occurring singly or in combination, that sometimes cause discharges at or below 10 kV. One of the problems arises after the source has been out of the vacuum for more than an hour or two. A spontaneous, gradual increase in anode current begins soon after the onset of electron bombardment of the anode. It continues, at an increasing rate, until halted by intervention of the overcurrent trip mechanism of the high voltage power supply. This phenomenon is caused by outgassing within the x-ray source.

Three precautions are useful in avoiding the outgassing problem: first, minimizing the duration of exposure to the atmosphere; second, allowing a sufficiently long warm-up period during which the accelerating

voltage is kept low; and third, storing the lava insulator in a dessicator or baking it in an oven at 100°C, if the source must be out of the vacuum for more than a few hours. The effectiveness of the third precaution indicates that water adsorbed on the lava insulator is the main contributor to the outgassing problem.

The other type of high voltage difficulty is characterized by the occurrence of "microdischarges," which are observable as tiny jumps in the anode current. Microdischarges are troublesome because they usually introduce extraneous counts into the recorded spectrum. Also, they are often followed by a spark that is large enough to cause an overcurrent trip. These symptoms are probably due to the existence of tiny projections on the anode or the grounded metal surfaces near the anode. Surface contamination of the insulator can produce similar results. If microdischarges occur during an experiment, it is sometimes possible to complete the run at a lower accelerating voltage. Before the source can again be operated at its optimum level, however, the above-mentioned surfaces must be cleaned and polished The polishing is best done on a lathe, using emery cloth or rouge and finishing with a polishing compound such as Met-all Formula 1187. The freshly polished parts are rinsed with acetone before being reassembled.

While the above precautions are necessary to keep the new x-ray source operating at 10 kV, it may be possible to push the limit even higher. The effect of a particular increase in the voltage can be calculated, using the empirical x-ray intensity-voltage formula (Eq. 2.1), coupled with the average value of the exponent determined from photoelectron counting rate data (1.80). Such a calculation predicts, for example, a 22 percent increase in counting rate if the source is operated at 12 kV rather than 10 kV and the power level is constant. Data given by Carlson [21] show a 15 percent increase under similar circumstances.

Power Dissipation

The most power that has been used for x-ray production in the new source is 108 watts. This level was achieved by bombarding a one-piece aluminum anode (of the type shown in Figure 2) with a current of 12 mA accelerated through 9 kV. A neon 1s photoelectron spectrum was recorded under these conditions. However, the anode current became unstable after about 10 minutes and visual examination of the anode confirmed that a small amount of sputtering had occurred at the x-ray generation site. The power limit for that anode is thus slightly less than 108 watts.

The optimum power for XPS experiments, about 80 W, is significantly less than the power limit. This margin of safety is necessary so that a power increase because of a

spontaneous change in filament position or sample gas pressure will not result in destruction of the anode.

According to the argument presented in Chapter II, the power limit is essentially equal to the maximum rate of heat removal from the anode. This rate is equal to $\Delta T_{max} \div R_{total}$ [22], where ΔT_{max} is the maximum temperature difference between the x-ray generation site and the cooling water, and R_{total} is the thermal resistance of the heat-flow path.[4] This resistance depends on the length L, area A, and thermal conductivity k of the path, according to the formula $R = L/Ak$ [25]. R_{total} may be described as the sum of three components: the resistance between the x-ray generation site (at the surface) and the bulk of the anode tip, which is significant because of the small area of the x-ray generation site; the resistance of the stem; and the resistance between the anode base and the cooling water, which is probably small because of the relatively large area of the path. Assuming that ΔT_{max} is approximately equal to the difference between the melting point of the anode material and room temperature, an experimental value of R_{total} can be determined. For the aluminum anode with a power limit near 108 W, R_{total} is about 5.9 kelvin per watt.

---

[4] Heat transfer by radiation and by residual-gas conduction are neglected; each is estimated [23, 24] to account for less than one watt of heat transfer from an aluminum anode at its power limit.

From the known thermal conductivity of aluminum, the resistance of the stem alone is 3.7 K/W, or 63 percent of the total.

Three possible approaches to increasing the power limit are evident in the above results: changing the dimensions of the stem to decrease its thermal resistance; increasing the conductivity of the stem by making it out of copper; and increasing the area of the x-ray generation site. The third approach is difficult in practice, since the area of the x-ray generation site can neither by controlled in a straightforward way nor observed directly. Changing the dimensions of the stem is more promising, but necessitates redesigning more than just the anode. This approach is discussed below, under Future Development.

The idea of using copper for the anode stem and base was investigated experimentally, employing the screw-on tip design shown above (sketch B, p. 8). Several aluminum anode tips were destroyed (by large-scale sputtering or even by bulk melting) during the course of XPS experiments. The power level at which this occurred varied considerably, but such anodes have not been used successfully at more than 45 W. However, a one-piece aluminum anode of the same dimensions has been operated for several hours at 49 W, without sustaining any damage. The thermal resistance of the tip-stem interface thus offsets the 65 to 70 percent conductivity advantage of copper over aluminum. The

observed variation in the power limit is probably attributable to differences in the actual contact achieved between aluminum tips and the copper stem. Chemical effects of the gaseous samples also may have contributed to the variation.

Anode Materials Other than Aluminum

The selection of the anode material (for a non-monochromatized x-ray source for XPS) is dictated by the energy and width of its characteristic x-rays and by other pertinent properties of the material, such as thermal conductivity and chemical stability. Aluminum is the most generally applicable anode material for XPS; however, the specific requirements of some experiments make the use of a different anode material necessary or at least desirable.

The measurement of chemical shifts in core ionization potentials often involves closely-spaced peaks, i.e., peaks whose separation is not much larger than their full width at half maximum. In such cases it may be advantageous to use magnesium as the anode material, since the Mg $K\alpha_{1,2}$ linewidth is less than that of Al $K\alpha_{1,2}$. Magnesium anodes have been used frequently in the new x-ray source to exploit the linewidth advantage.

Since the melting points of magnesium and aluminum are essentially the same, the ratio of their thermal conductivities (0.65 Mg:Al) should approximately equal the ratio of the power limits of one-piece magnesium and aluminum anodes.

Thus the power limit of a 7.9 mm-diameter, one-piece Mg anode should be about 0.65 times the 108 W limit of a similar Al anode, or 70 W. Such a magnesium anode has been operated at 36 to 40 W for many hours and at 50 W for two hours without any indication of damage. Magnesium tips mounted on the copper stem have also been used successfully; however the power limit varies widely for individual Mg tips, as it does for Al tips. The highest power level that has been achieved with a Mg tip anode is 34 W. XPS experiments over ten hours in duration have been carried out at 21 W.

The difference between the resolution of closely-spaced photoelectron peaks due to Al $K\alpha_{1,2}$ and Mg $K\alpha_{1,2}$ radiation is of sufficient magnitude to be apparent from casual observation of similar spectra. It should be noted, however, that the uncertainties of core ionization energies measured with Al $K\alpha_{1,2}$ radiation may be less than the uncertainties of similar measurements with Mg $K\alpha_{1,2}$ if there are many more counts in the former spectrum than in the latter. Since aluminum anodes can produce higher photoelectron counting rates,[5] it is thus advisable to use Al $K\alpha_{1,2}$ radiation even for closely-spaced peaks if getting

---

[5]This is true because of the 36 percent greater attenuation of Mg x-rays in the Al foil window [26] and the difference in optimum power levels. Two smaller effects favor Mg: greater cross section for photoionization (about 15 percent for carbon [27]), and greater x-ray generation efficiency (about 6 percent at 10 kV).

enough counts is expected to be difficult. This would be the case if the amount of sample material were very limited, or if low-intensity features such as "shake-up" peaks were to be observed, or if time itself were a limiting factor.

Another anode material of some interest is titanium. Ti $K\alpha_{1,2}$ radiation, consisting of two broad peaks at 4510.92 eV and 4504.94 eV [15, 16], can be used to produce photoelectron and Auger spectra that require more than the Al $K\alpha_{1,2}$ energy. The tip-stem anode design is ideal for titanium: its thermal conductivity is a factor of 19 less than that of copper. Because of its high melting point, however, the power limit of the Ti tip mounted on the copper stem is nearly 80 W. Ti $K\alpha_{1,2}$ radiation has been employed to generate the KLL Auger and 1s photoelectron spectra of argon. An attempt to produce a carbon 1s photoelectron spectrum using Ti $L\alpha_{1,2}$ x-rays was unsuccessful. With an energy of 452.2 eV [15], these x-rays are very strongly attenuated by the aluminum window.

Copper has also been used as an anode material in the new x-ray source. Specifically, a copper tip mounted on the copper stem was employed to produce neon Auger and photoelectron spectra due to CuL x-rays. The Auger spectrum was noteworthy because of the excellent signal-to-background ratio, 148:1. The energy of Cu $L\alpha_{1,2}$ radiation is 929.7 eV [15],; the resulting kinetic energy of neon 1s photoelectrons is about 60 eV. The full width at half maximum of the

neon 1s spectrum was about 2.7 eV, this being almost entirely attributable to the width of the Cu $L\alpha_{1,2}$ radiation.

Filament Operation

The full-wave-rectified, filtered power supply designed to heat the filament of the original x-ray source provides insufficient power for the much longer filament of the new source. An AC power supply (Variac and step-down transformer) was substituted. The filament is heated with a current of 5-6 amperes at 6-8 volts (rms).

The possible adverse effects of the magnetic field generated by the filament current were a matter of concern, especially since early spectra for which the new x-ray source was used were somewhat broader than expected and slightly asymmetric. The following experiments involving neon Auger spectra failed to disclose any magnetic field effects. A bifilar filament, arranged so the net magnetic field would be very small, made no apparent difference in the spectrum, nor did the use of full-wave-rectified heating current. No significant change was observed even when half-wave-rectified heating current and an anti-coincidence circuit were employed, allowing counts to be recorded only during the "off" half of the heating current cycle. The spectrometer resolution was later determined to be much more dependent on the cleanliness of the graphite-coated

surfaces of the sample cell than on the choice of x-ray source.

Since the filament is over 8 cm long, supported only at the ends, and held in a nearly circular configuration, it is subject to considerable distortion while in operation (at a temperature on the order of 1800°C). On rare occasions the filament has actually been short-circuited by touching the wall or floor of the filament chamber. More commonly the distortion is small, but not insignificant. An upward distortion tends to increase both the anode current and the rate of tungsten deposition on the anode. If the filament flexes downward, the anode current decreases, sometimes to the extent that the normal anode-current level cannot be restored, even by a dramatic increase in filament current.

In the latter case, the voltage gradient in the vicinity of the filament is significantly reduced. This causes inefficient acceleration of the electrons toward the anode, and a space charge builds up. The anode current thus becomes quite insensitive to the filament temperature. However, by applying a small, negative bias voltage to the filament, the necessary voltage gradient can be restored and the operation of the filament returned to normal. There is a threshold, dependent on both the heating current and the position of the filament, below which the use of a bias voltage depresses the anode current. At the threshold,

the bias voltage has no effect at all. Beyond the threshold, the magnitude of the optimum bias voltage increases gradually. A bias of more than 10 volts is seldom necessary.

Future Development

Considerable thought has already gone into the possible design of another all-new x-ray source for the OSU spectrometer, which would include such features as a directly-cooled anode and provision for irradiating high-temperature vapor samples. Nevertheless, the present x-ray source is likely to be used for routine gas-phase XPS measurements for many months to come. It is therefore appropriate to continue to modify this source to apply the ideas which have arisen from operational experience and to exploit the other changes being made in the XPS instrument.

Recently a new filament power supply has been put into use, which stabilizes the anode current by means of adjustable current and voltage limits and a feedback circuit specially designed by T.D. Thomas. This development will allow the optimum power level for each type of anode to be raised closer to the corresponding power limit. An increase of up to 20 percent may be possible.

Another change, soon to take place, is the installation of a separate pumping system to maintain the vacuum in and around the x-ray source. Several benefits are expected to

result from this development. Because the x-ray source region will be sealed off from the rest of the spectrometer, much larger pump-out holes in the source can be used without allowing many extraneous electrons to reach the detector. The pressure in the x-ray source will thereby be reduced, the outgassing problem lessened, and perhaps the accelerating voltage limit (x-ray generation efficiency) will be increased. Further improvement could be obtained by replacing the lava insulator with a less absorptive material and the brass filament supports with a metal of lower vapor pressure.

As was concluded in the above discussion of power dissipation, redesigning the x-ray source to accommodate a shorter, thicker anode is the most promising approach to raising the power limit. Preliminary sketches indicate that the length of the anode can be reduced by about a factor of two and its cross-sectional area increased by a factor of 2.6 if certain other design changes are also implemented. These include changes in the method of supporting the filament and the method of holding the main parts together, which would enable the use of a shorter filament chamber and main insulator. A 25 percent increase in the diameter of the window and in the inside diameter of the central cylinder would also be necessary.

By virtue of the greater conductance of the anode stem, implementation of these modifications of the x-ray source design would increase the power limit by a factor of two, even if there were no change in the thermal resistance of the x-ray generation site. The latter would probably decrease, however, because of the much greater surface area of the tip of the new anode. The new power limit would thus be at least twice as great as the present limit, or more than 200 watts for a one-piece aluminum anode.

PART TWO

GAS PHASE XPS OF COMPOUNDS CONTAINING MULTIPLY-BONDED OXYGEN

V. INTRODUCTION

From the first reported observation of chemical shifts in core-level photoelectron spectra [28] in 1958, until at least 1973, the interpretation of such shifts was sought almost exclusively in terms of differences in initial-state charge distribution. Potential models were employed for the computation of ground-state charge distributions from measured chemical shifts [29], and series of molecules to be studied were often chosen so any final-state effects would be likely to cancel out. However, by the time the International Conference on Electron Spectroscopy was held in Namur, Belgium, in April, 1974, a change of emphasis was becoming evident. This led Carlson to comment in the Summary Talk at Namur [30]

> Photoionization is a description of a phenomenon which proceeds from an initial to a final state. It is as though we have been looking at half the problem all the years; now the other half is receiving its proper attention.

Shirley, in a review (given at Namur) of the relation of XPS results to other physical and chemical data [31], stated that while the core ionization energy shift

> depends on both initial- and final-state effects, so also does the reactivity, and in the same way. This is a positive feature of ESCA shifts, because reactivity is, after all, the quantity of real interest to the chemist.

In Part Two, the techniques and results of a gas-phase XPS study of eleven esters, four acids, acetone, and carbon monoxide are presented. The latter was included primarily because of its utility as a calibrant, but the measured core ionization energies have also been employed to evaluate the accuracy of some recent theoretical work on CO. The carbon 1s and oxygen 1s ionization energies of the other molecules have been used to assess the relationship of such energies to some other measures of gas-phase chemical reactivity, namely, proton affinity and gas-phase acidity, as well as σ and π electronegativity of substituents on carbonyl compounds. New chemical information was obtained on the basis of each of these relationships.

VI. EXPERIMENTAL PROCEDURES AND DATA ANALYSIS

Source and Purity of Sample Compounds

All of the compounds used in this study were obtained commercially.[6] With four exceptions, they were indicated by the supplier to be at least 97 percent pure. The purity of three compounds was indicated indirectly: the ethyl acetate was "analytical reagent" grade, while the methyl formate and ethyl formate were characterized by their boiling point ranges, 31.5-32.5°C and 53-54°C, respectively. Further purification was carried out on just one compound, formic acid. It was an "analytical reagent" with a guaranteed assay of 88 percent; an NMR spectrum confirmed the presence of a significant amount of water. The formic acid was dried by refluxing for six hours with a molar excess of phthalic anhydride and recovered by distillation. An NMR spectrum of the dried formic acid indicated that the water had been effectively removed.

Procedures for Generating Photoelectron Spectra

Carbon 1s and oxygen 1s photoelectron spectra were obtained using the Oregon State University Cylindrical Electrostatic Analyzer with the new x-ray source described

---

[6]The suppliers were Aldrich, Mallinckrodt, Matheson Coleman and Bell, Matheson Gas Products, and PCR.

in Part One. Gaseous samples and calibrants entered the system separately through the stainless steel needle valves of a gas inlet manifold, then passed through a long copper tube to the sample cell. The calibrants and samples stored in pressurized cylinders were connected to the inlet manifold by way of a regulator valve. The samples that are liquids at room temperature were mounted in a glass ampule attached directly under a needle valve. The rates of flow were adjusted to provide a total pressure in the sample cell of 0.08 to 0.1 torr as measured by a McLeod gauge. For some experiments involving the less volatile liquids, the total pressure was as low as 0.05 torr. A heating tape was employed to minimize the pressure fluctuations that sometimes occurred due to condensation in the needle valve.

The duration of individual experiments ranged from less than three hours to well over 24 hours, depending on the method of calibration, the sample pressure, and the spacing of the peaks to be resolved, as well as on x-ray source performance. For most experiments, a collimator shield was employed to minimize background features in the carbon 1s and oxygen 1s regions. The focusing voltage was measured at a channel near the tip of each peak, using a highly accurate differential voltmeter (Julie Research Labs Model TD-1000). The peak positions were determined by least-squares fitting (discussed in a following section),

and the focusing voltages were corrected to correspond to these positions. With a few exceptions,[7] each reported ionization energy represents the combined results of two or more spectra. Many of the ionization energies were measured with both Al $K\alpha_{1,2}$ and Mg $K\alpha_{1,2}$ radiation.

Energy Calibration

For electrons entering the electrostatic analyzer at a non-relativistic velocity,[8] the required focusing voltage V is related to their kinetic energy K by the simple expression

$$V = CK + B. \qquad \text{(Eq. 6.1)}$$

The spectrometer constant C has been calculated from the dimensions of the spectrometer to be 0.8019 ± .0002 V/eV [12]. Even though no initial retarding potential is applied in the OSU instrument, a small offset voltage B is observed. The offset voltage affecting gas-phase measurements is partially attributable to the presence of positive ions in the sample cell [32]. The offset voltage is sensitive to the cleanliness of the graphite-coated sample

---

[7] Only one measurement each was made for carbon 1s in ethyl formate, ethyl acetate, ethyl difluoroacetate, methyl trifluoroacetate, and trifluoroacetic acid, also oxygen 1s in ethyl trifluoroacetate.

[8] The correction applied for relativistic effects is discussed below under Computation of Accurate Ionization Energies and Uncertainties.

cell and collimator surfaces, indicating that surface charging also contributes significantly. Neither B nor C is sufficiently constant over time to allow an accurate kinetic energy to be calculated from a single measured focusing voltage: it is necessary to calibrate each spectrum while it is being recorded.

The energy calibration methods employed in this study were based on the neon 1s ionization energy (870.312 ± .017 eV) determined by Thomas and Shaw [14], and on the neon 2s ionization energy (48.476 ± .002 eV) known from optical spectroscopy [33,15]. Neon calibration was usually accomplished by recording the neon 1s and neon 2s photoelectron peaks along with the oxygen 1s or carbon 1s spectrum (or both) from a mixture of neon and sample gas. In a few cases, the neon $^1D_2$ Auger peak was used instead of the much less intense neon 2s peak.[9] The focusing voltage was controlled and the data collected and stored by an interfaced PDP-9 computer, which was programmed to allow successive scanning of up to four operator-selected energy regions. Each series of scans took one or two minutes; most experiments incorporated several hundred scans of each retion. The nominal channel width was 0.1 volt. The measured focusing voltages and known energies of the neon

---

[9] See further discussion of this method below, under Uncertainty Analysis.

peaks sufficed to determine both C and B, allowing the energy corresponding to each sample peak to be computed.

Many of the spectra in this study were calibrated by a simpler approach, the internal method, in which sample peaks were recorded simultaneously with a single, nearby peak from a calibrant. Measuring energies relative to a calibrant peak eliminated the need to determine the offset voltage B; and, since the energy differences were always less than ten electron volts, an approximate spectrometer constant could be used without contributing to the uncertainty of the measurement. The relative energies thus determined were convertible to absolute ionization energies because the calibrant peaks had previously been measured by the neon method. CO_2, with ionization energies of 297.71 ± .05 eV (carbon 1s) and 541.32 ± .05 eV (oxygen 1s) [14], was employed as an internal calibrant for many carbon 1s spectra and for the oxygen 1s spectrum of CO. The core ionization energies of CO were determined from a combination of neon- and CO_2-calibrated spectra (see Chapter VII), and CO was subsequently used as an internal calibrant for oxygen 1s spectra of several other molecules. The multichannel analyzer and accompanying electronics described in reference 12 were used to control the focusing voltage and to collect and store the data for internally-calibrated spectra.

Least-Squares Fitting

The positions of the photoelectron peaks were determined by least-squares fitting with computer programs employing gaussian peak-shapes and a linear background. The fitting was originally done without any constraints. Unfortunately, this approach proved to be inadequate for fitting closely-spaced peaks, as is illustrated by the preliminary results for ethyl chloroacetate. This molecule, like the other esters and acids observed in this study, should have an oxygen 1s spectrum consisting of two peaks of equal intensity (area), representing the two chemically inequivalent oxygen atoms. The two peaks are about 1.4 eV apart in the ethyl chloroacetate spectra; the corresponding separation ranges from 1.3 to 1.8 eV for the other esters and acids. The left half of Table 1 shows the area ratio of the two oxygen 1s peaks and the greater of the two corresponding ionization energies from three separate ethyl chloroacetate spectra. Since the spectra were neon-calibrated, there was no internal-calibrant peak to complicate the fitting. Each spectrum was fit without constraint. The area ratios vary widely, and the difference between the ionization energies from the first two spectra is well beyond the sum of their uncertainties, which are shown in parentheses.

Table 1. Comparison of unconstrained fitting with area-ratio-constrained fitting.

Spectrum Number	Unconstrained		Area-Ratio-Constrained	
	Area Ratio	Ioniz. Energy, eV	Area Ratio	Ioniz. Energy, eV
1	0.58	539.67 (12)	1.00	539.54 (4)
2	1.67	539.33 (12)	1.00	539.49 (5)
3	0.98	539.53 (12)	1.00	539.52 (4)
mean of 1,2,3		539.51 (7)		539.52 (3)

A more versatile least-squares program was obtained[10] and used to fit the same spectra with gaussian peak-shapes and a linear background and with the areas of the two oxygen 1s peaks constrained to be equal. As shown in the right half of Table 1, the differences among the three resulting values of the ionization energy are well within the sum of their uncertainties, even though the uncertainties themselves are much smaller than before. The range of the three ionization energy values from unconstrained fitting is 0.34 eV, while the corresponding range from the fits with constrained area ratios is 0.05 eV. It is strictly coincidental that the mean values are almost identical; the constraining of known area ratios did cause significant shifts in several of the other ionization

[10] The program GAMET was provided by B.E. Mills of Lawrence Berkeley Laboratory.

energies reported in this study. All the spectra whose unconstrained area ratios differed by five percent or more from the stoichiometric values were refit with the known area ratios constrained. The area ratios of the carbon 1s peaks in ethyl acetate, ethyl chloroacetate, and ethyl bromoacetate were constrained to be 1:1:2, 1:2:1, and 1:2:1, respectively (with ionization energy decreasing to the right). While the two carbon atoms represented in each double-intensity peak are not located in equivalent sites, their ionization energies are so nearly equal that these composite peaks have about the same width as the accompanying single peaks.

Computation of Accurate Ionization Energies and Uncertainties

In determining core ionization energies accurately -- to within a few hundredths of an electron volt -- it is necessary to account for relativistic effects and for the recoil energy of the molecular ion. A formula derived by Thomas and Shaw [14] was used to compute the required corrections for relativistic effects. The absolute corrections to the kinetic energies of oxygen 1s and carbon 1s photoelectrons ejected by Al $K\alpha_{1,2}$ x-rays were about 0.10 eV and 0.16 eV, respectively. These were largely offset by similar correction of the calibrant kinetic energies, however. The net relativistic corrections were .018 eV and

.015 eV, respectively, with neon 1s-2s calibration, and were completely negligible with internal calibration.

The magnitude of the kinetic energy of the recoiling molecular ion ranged from 0.023 eV for carbon 1s and 0.018 eV for oxygen 1s in CO, the lightest sample molecule, to 0.003 eV for oxygen 1s in ethyl bromoacetate, the heaviest. The recoil corrections were thus quite small, but not necessarily negligible -- even with internal calibration.

The ionization energies reported in this study were each based on a small number of individual spectra (two, three, or four in most cases). As a consequence, the distribution of the individual measurements of each energy was considered to be of little statistical significance and not necessarily indicative of the actual uncertainty of the resulting mean value. To determine the realistic uncertainty of individual ionization energy measurements and of the weighted-mean values to be reported, all of the possible sources of error were listed, then recategorized where necessary, into uncorrelated components. The total uncertainty was computed by applying a formula [34] that can be written in the general form[11]

$$\sigma_x^2 \simeq \Sigma_v [(\partial x/\partial v)^2 \sigma_v^2]. \qquad \text{(Eq. 6.2)}$$

---

[11] The approximations inherent in this formula require that the individual sources of error be uncorrelated and that the error in each parameter be small compared to the range of that parameter. Both conditions are met in this case.

The uncertainty contribution from each uncorrelated source of error was thus weighted according to the sensitivity of the ionization energy to changes in that parameter.

For convenience, the sources of calibration error and experimental error were grouped, such that

$$\sigma_E^2 = \sigma_{cal}^2 + \sigma_{expt}^2 \qquad \text{(Eq. 6.3)}$$

where σ_E represents the total uncertainty in the ionization energy. The methods of computing σ_{expt} and the uncertainties of weighted-mean ionization energies are presented in Appendix A. For the internally-calibrated spectra, σ_{cal} is equal to the uncertainty of the known ionization energy of the calibrant peak. Three uncorrelated sources of error were found to be inherent in Ne 1s-2s calibration: the uncertainty of the Al $K\alpha_{1,2}$ x-ray energy, the experimental uncertainty in the neon 1s-Auger energies determined by Thomas and Shaw [14], and the uncertainty of the neon 2s ionization energy, which is negligibly small. These three also underlie the other method of neon calibration, using the neon 1s and $^1D_2$ Auger peaks, but with this method the uncertainty of the Mg $K\alpha_{1,2}$ x-ray energy also enters in when that radiation is employed.

The coefficients of these uncertainty components vary with the sample ionization energies in different ways for the two methods of neon calibration because the known values of the Ne 1s and Ne 2s energies are essentially

independent of one another, but the Ne 1s and Ne Auger energies are not [14]. Figure 3, a graph of calibration uncertainty versus ionization energy, illustrates the differences. The Ne 1s-2s calibration is essentially independent of the energy (and thus the uncertainty) of the x-radiation that is employed. However, Ne 1s-Auger calibration depends on the x-ray energy (and its uncertainty) because the 1s photoelectron kinetic energy varies with x-ray energy while the Auger kinetic energy does not. The Ne 1s-Auger calibration uncertainty with Mg $K\alpha_{1,2}$ x-rays is less than with Al $K\alpha_{1,2}$ at most energies because the two points span an energy region over twice as wide in the former case as in the latter. Ne 1s-2s calibration gives the lowest uncertainties at most energies. In fact, the only 1s spectrum in the region where Ne 1s-Auger is best is that of fluorine, and it is usually measured by internal calibration relative to neon Auger (with Al $K\alpha_{1,2}$ x-rays). The one redeeming characteristic of Ne 1s-Auger calibration, mentioned previously, is that it takes about half as much time as Ne 1s-2s. As shown in Figure 3, the Ne 1s-Auger calibration uncertainty is reasonably close to that of Ne 1s-2s in the oxygen 1s region: this is where the former method is most useful, especially if Mg $K\alpha_{1,2}$ radiation is required.

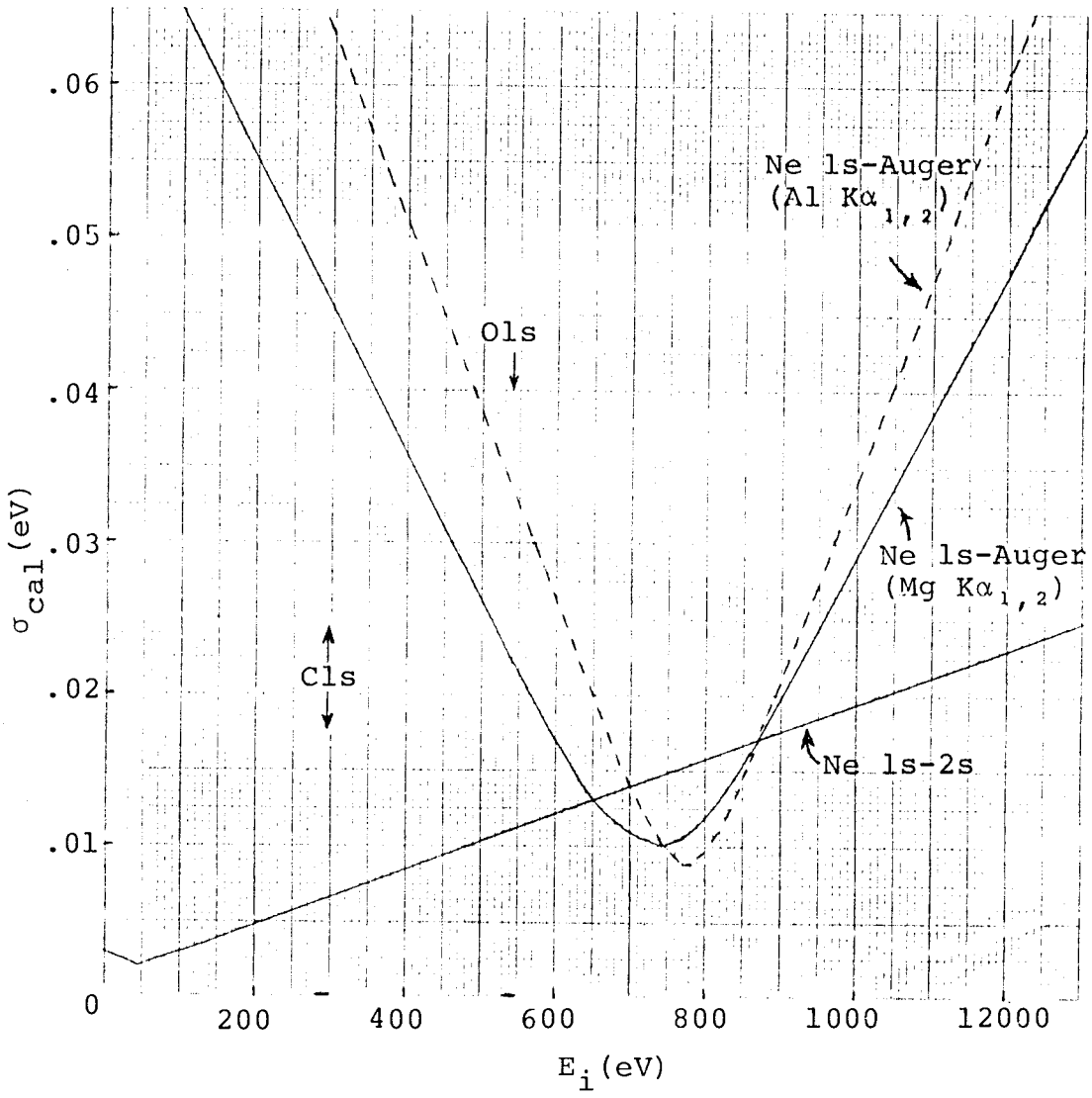

Figure 3. Inherent uncertainty in neon calibration as a function of ionization energy.

VII. CORE IONIZATION ENERGIES IN CARBON MONOXIDE

Accurately measured values of the core ionization energies of carbon monoxide are of both experimental and theoretical significance. The theoretical significance has come about because sophisticated quantum-mechanical techniques have been employed for investigation of the carbon monoxide molecule. Hartree-Fock calculations with large basis sets have been reported for the neutral molecule and also for the oxygen 1s and carbon 1s core-hole states. Since these represent the initial and final states for core ionization, the difference in total energy between the neutral-molecular ground state and each core-hole state constitutes a theoretical ionization energy. These, and other, less-sophisticated calculations, can best be judged in comparison with accurately-measured values.

From an experimental point of view, the oxygen 1s photoelectron peak from carbon monoxide is particularly useful for internal calibration. It is separated by more than two electron volts from the oxygen 1s peaks of most organic, oxygen-containing molecules; and, it is not complicated by multiplet splitting as are the NO and O_2 spectra. The carbon 1s photoelectron peak from carbon monoxide has also been employed for internal calibration.

In an article published recently and included below as Appendix B, the author and T. Darrah Thomas [35] reported accurately measured core ionization energies for carbon monoxide: 542.57 ± .03 eV (O1s) and 296.24 ± .03 eV (C1s). The experimental values that had been reported previously ranged over 0.5 eV (O1s) and 0.4 eV (C1s) with individual uncertainties of at least 0.1 eV. Four sets of theoretically calculated 1s ionization energies for CO were listed and discussed in comparison with the new experimental results. Calculations of near-Hartree-Fock accuracy [36] predicted an oxygen 1s value about 1 eV lower than experiment and a carbon 1s value about 0.5 eV higher than experiment. These differences were qualitatively accounted for in terms of correlation energy effects.

VIII. CORRELATION OF CORE IONIZATION ENERGIES WITH PROTON AFFINITIES

Early Studies

In 1974, Martin and Shirley [38] pointed out the notable similarity between the core ionization process

$$A \rightarrow A^{*+} + e^{-} \qquad \Delta H = E_i \qquad \text{(Eq. 8.1)}$$

(where the asterisk represents a core hole) and the protonation process

$$A + H^{+} \rightleftarrows AH^{+} \qquad \Delta H = -PA \qquad \text{(Eq. 8.2)}$$

When A is an alcohol, for example, core ionization of the oxygen atom and protonation both result in a final state with an excess positive charge at or near the oxygen atom. On the basis of this analogy, Martin and Shirley anticipated a close correspondence between the chemical shifts ΔE_i(O 1s) and $-\Delta PA$[12] for the alcohol series H_2O, CH_3OH, CH_3CH_2OH, $(CH_3)_2CHOH$, and $(CH_3)_3COH$. They tested the relationship by plotting experimental ionization energy shifts relative to H_2O for the above series and for CF_3CH_2OH against the corresponding proton affinity shifts as determined by ion cyclotron resonance studies [39]. A

---

[12] The minus sign reflects the conventional definitions of proton affinity and ionization energy shown in Eq. 8.1 and Eq. 8.2.

striking correlation of ΔE_i and $-\Delta PA$ was found: the data were fit quite well by a straight line of unit slope. A similar correlation was demonstrated using ΔE_i (N 1s) and $-\Delta PA$ for the methyl-substituted amines CH_3NH_2, $(CH_3)_2NH$, and $(CH_3)_3N$ relative to NH_3. Martin and Shirley concluded that the $\Delta E_i = -\Delta PA$ relation would probably be valid for a wide range of substituted alcohols, but that it was less likely to hold for other oxygen-containing molecules, such as acids.

In an article published simultaneously with that of Martin and Shirley, Davis and Rabalais [40] developed a potential energy model employing CNDO/2 wave functions to calculate proton affinities. By comparison of this model with potential energy models that have been devised for core ionization energy calculations, they were able to rationalize the observed linear correlation of ΔE_i and $-\Delta PA$. Davis and Rabalais plotted E_i versus PA (experimental values) for some alcohols and amines, illustrating the linear correlation. They also plotted data for two molecules containing doubly-bonded oxygen, HCOOH and CH_3COCH_3, but neither of these fit the correlation. This observation was qualitatively accounted for on the basis of trends apparent in the potential model calculations.

Extension to Molecules Containing Doubly-Bonded Oxygen

The work of Martin and Shirley and of Davis and Rabalais raised the interesting possibility that the chemical shifts in core ionization energies and proton affinities are of similar magnitude for a wider range of compounds than they were able to test. Since the oxygen 1s ionization energies of CO_2 and H_2CO (previously measured in this laboratory) were found to fit the correlation, the measurement of other compounds containing doubly-bonded oxygen was undertaken.

The early results of this project proved to be quite significant: the correlation held with unit slope for four additional compounds, CH_3CHO and CH_3COCH_3 (measured by T. X. Carroll) and HCOOH and CH_3COOCH_3[13] (measured by the author). The oxygen 1s ionization energies for CH_3CHO, CH_3COCH_3, and HCOOH differed significantly from previously reported values.

This extension of the $\Delta E_i = -\Delta PA$ relation was reported by T. X. Carroll, the author, and T. D. Thomas [41] in an article that is included below as Appendix C. Three

---

[13] The E_i (O 1s) values for CH_3COCH_3, HCOOH, and CH_3COOCH_3 used in this correlation were preliminary results. For CH_3COCH_3, only a single measurement had been made. For the other two, the techniques of area-ratio-constrained fitting and uncertainty-weighted averaging had not been employed. Final results reported later in the chapter differ by 0.03-0.08 eV.

significant conclusions were reached on the basis of the extended correlation. First, compounds containing doubly-bonded oxygen fit the correlation as well as those containing only singly-bonded oxygen, but the two groups are separated from each other by about 0.25 eV. Such a hybridization effect was anticipated by Davis and Rabalais [42]. Second, for HCOOH and for CH_3COOCH_3 the lower of the two E_i (O 1s) values fits the correlation. These were unambiguously identified as the doubly-bonded-oxygen values by comparison with the spectrum of $(CH_3O)_2CO$, in which the two peaks differ by a factor of two in intensity. Third, since the $\Delta E_i = -\Delta PA$ relation relies on close proximity of the core ionization site and the protonation site, gas phase protonation of these molecules must occur at the doubly-bonded oxygen. On the other hand, Pesheck and Buttrill [43] concluded from ion cyclotron resonance (ICR) studies that the gas-phase protonation of esters occurs at the singly-bonded oxygen. However, more recent ICR work [44] supports our conclusion.

The success of the above extension of the core ionization energy-proton affinity correlation contributed to the decision to continue the XPS investigation of acids and esters in this laboratory. Halogenated molecules were emphasized in order to test the correlation for several cases involving large inductive effects.

While this work was in progress, Mills, Martin, and Shirley [45] published a comprehensive study of the correlation of chemical shifts in core ionization energies and proton affinities, including measurements for 23 oxygen-containing compounds, 16 amines, 4 phosphines, and 3 sulfides. With the single exception of CF_3COOH, the members of each series of related compounds (such as alcohols, acids, or amines) differed only by alkyl substitution. On the basis of the correlation observed for oxygen, Mills et al. reached the same three conclusions discussed above: namely, that separate correlations for singly- and doubly-bonded oxygen can be observed, that for acids and esters the doubly-bonded oxygen fits the correlation, and that it therefore provides the site of protonation in the gas phase.

Mills et al. [45] were able to make a more detailed analysis of the correlation for amines. The primary, secondary, and tertiary series each fall on a separate line having a slope of about 1.5, while the line through the initial members of those series, CH_3NH_2, $(CH_3)_2NH$, and $(CH_3)_3N$, had a slope of about 0.7. Nevertheless, a line of unit slope gave a reasonable fit to all the points in general.

The above analysis of the correlation for amines raises the possibility that more detailed information might also be found within the observed general correlation for molecules containing doubly-bonded oxygen. It has been argued by Martin and Shirley [38] and by Davis and Rabalais [40] that the relaxation component ΔR in the chemical shifts of proton affinities and core ionization energies (for the protonated atom) should be about equal in magnitude. That is, $\Delta R(PA) \approx \Delta R(O\ 1s)$. On the other hand, Davis and Rabalais found a trend in their CNDO/2 calculations indicating that inductive shifts ΔV (arising from differences in the ground-state charge distributions) should be larger for core ionization energy than for proton affinity. That is, ΔV (O 1s) > $\Delta V(PA)$. The correlation of Mills et al. [45] gives some indication of such an effect. Linear least-squares fits to their data for three relaxation-dominated series of molecules, HCOOR, CH_3COOR, and RCOOH (R = H, CH_3, C_2H_5; also C_3H_7 for esters), give slopes of 0.7, 0.7, and 1.1 respectively. The only shift that is clearly inductive in origin, defined by the CF_3COOH and CH_3COOH data, corresponds to a slope of about 1.4. However, these slopes were determined from only two to four data points each, and the proton affinities used have uncertainties of at least 0.1 eV. The existence of different slopes for the correlation of inductive and relaxation shifts therefore cannot be clearly established by reference to the data of Mills et al.

Reported in Table 2 are accurate, absolute core ionization energies for the doubly-bonded (carbonyl) oxygen in 17 organic compounds, including acids, esters, aldehydes, and acetone. Eleven of these values are from this work. For two additional acids, CFH_2COOH and $CClH_2COOH$, approximate values are listed. These acids were, respectively, not commercially available and not sufficiently volatile. The approximate ionization energies appearing in Table 2 were determined from measurements for the corresponding ethyl esters according to the formula

$$CXH_2COOH \approx \left(\frac{CF_2HCOOH - CH_3COOH}{CF_2HCOOC_2H_5 - CH_3COOC_2H_5}\right)(CXH_2COOC_2H_5 - CH_3COOC_2H_5) + CH_3COOH \qquad \text{(Eq. 8.3)}$$

where each molecular symbol represents E_i(O 1s) for the carbonyl oxygen in that compound.[14] As a test case, this method was used to estimate the value for CF_3COOH from the experimental value for its ethyl ester (with CF_3 replacing CXH_2 in Eq. 8.3): the result differed by only 0.01 eV from the experimental value for CF_3COOH.

Two new sets of experimental proton affinities have recently become available, each set determined from the equilibrium constants of an overlapping sequence of proton transfer reactions. One set was measured at 300K by the

---

[14] See Appendix D for a complete tabulation of the core ionization energies measured in this study.

Table 2. Experimental core ionization energies for doubly-bonded oxygen and experimental proton affinities.

Compound	E_i(eV)[a]	PA(eV)[f]	PA_{300K} (kcal/mol)[g]	PA_{600K} (kcal/mol)[h]
HCOOH	539.00(3)	7.80	179.8	178.6
CH_3COOH	538.29(2)	8.14	187.7	187.9
C_2H_5COOH	538.26(5)[b]	8.24	-	190.0
$CClH_2COOH$	538.68[c]	7.93	-	182.9
CFH_2COOH	538.76[c]	7.96	-	183.4
CF_3COOH	539.56(3)	7.51	173.0	170.8
$HCOOCH_3$	538.45(3)	8.13	187.4	187.5
CH_3COOCH_3	537.92(3)	8.46	195.1	195.1
CF_3COOCH_3	539.03(3)	7.81	180.0	-
$HCOOC_2H_5$	538.26(3)	8.28	190.9	190.9
$CH_3COOC_2H_5$	537.78(3)	8.58	197.8	197.7
$CF_3COOC_2H_5$	538.83(4)	7.93	182.9	-
$HCOOC_3H_7$	538.19(6)[b]	8.33	192.0	191.4
$CH_3COOC_3H_7$	537.78(6)[b]	8.60	-	198.2
$CH_3OCOOCH_3$	538.06(3)	8.54	196.9	-
H_2CO	539.44(6)[d]	7.56	174.3	-
CH_3CHO	538.62[e]	8.01	184.7	185.1
C_2H_5CHO	538.48(4)[b]	8.14	187.7	187.6
CH_3COCH_3	537.96(3)	8.40	193.6	193.5

[a] This work unless otherwise labelled. Uncertainty in the last digit is given in parentheses.

[b] Determined using shifts from reference [45] and the CH_3COCH_3 value from this work.

[c] Approximate values determined from shifts of corresponding esters. See text.

[d] Reference [46].

[e] Reference [41].

[f] PA_{300} value used when both PA_{300} and PA_{600} are available.

[g] Determined using proton affinity shifts at 300K from reference [44] and $PA(NH_3)$ = 202 kcal/mol from reference [47].

[h] Determined using proton affinity shifts at 600K from reference [48], with $T\Delta S$ (symmetry number) corrections added as in reference [44], and $PA(NH_3)$ = 202 kcal/mol from reference [47].

pulsed ion cyclotron resonance method [44] and the other at 600K by high-pressure mass spectrometry [48]. Pertinent values from each set are listed in Table 2, having been converted from shifts relative to NH_3 by using $PA(NH_3)$ = 202 kcal/mol [47]. The shifts from reference [48] were first converted from ΔG to ΔH (as was done in reference [44]), assuming that entropy changes other than those due to changes in rotation symmetry numbers were negligible.

It should be noted that while the two new sets of proton affinities are in good agreement with each other, they differ markedly from the previously reported values upon which the correlations of Carroll et al. [41] and Mills et al. [45] relied. The total range of the new proton affinities is nearly 40 percent less.

The core ionization energies and proton affinities (converted to eV) listed in Table 2 are plotted in Figure 4. A good, general correlation of ΔE_i and ΔPA is observed, but the slope is now -1.6 ± .1 instead of the previously reported unit slope. The absolute core ionization energies measured in this study are plotted as filled circles; the line is a linear least-squares fit to these points. Other data from Table 2 are represented by open circles. In all, only two points, corresponding to CH_3COOH and $CH_3OCOOCH_3$, fall more than 0.1 eV off the line. The reported accuracy of the proton affinity shifts is about 0.2 kcal/mol or 0.01 eV.

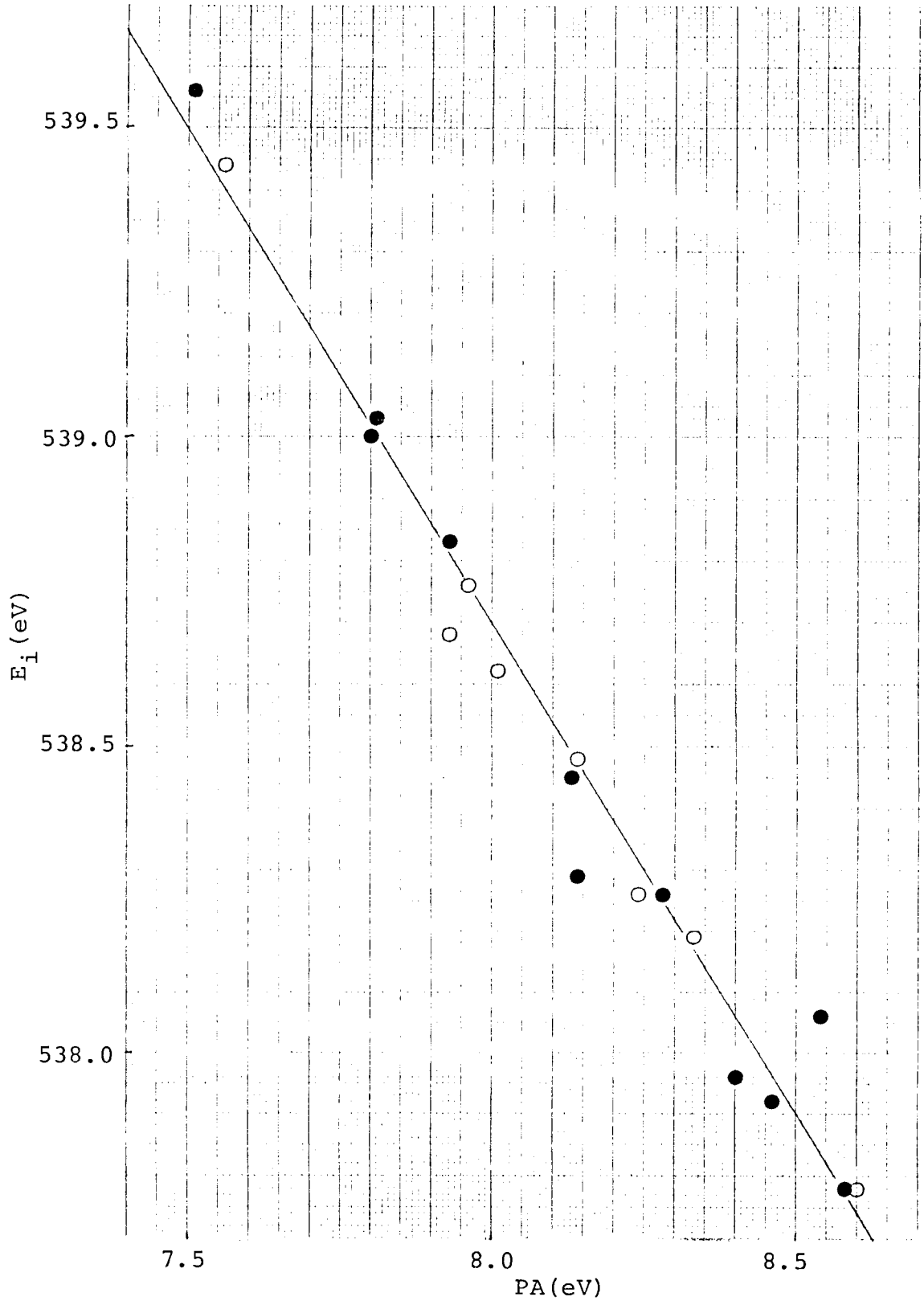

Figure 4. Correlation of core ionization energy with proton affinity for doubly-bonded oxygen.

The slope of the new correlation line is at odds with the theoretical work of Davis and Rabalais [40], as well as with the intuitive thinking reported in the other previous articles on this subject. The slopes observed for the small series of related molecules HCOOR, CH_3COOR, CF_3COOR, and RCOOH are -1.5, -1.1, -1.7 and -1.9, respectively. The slopes corresponding to the CF_3COOR-CH_3COOR shifts for the acids, methyl esters, and ethyl esters are -2.0, -1.7, and -1.6 respectively. The concept of distinct slopes characteristic of relaxation shifts and inductive shifts is thus not supported by the new results. The uncertainties of individual slopes are still rather large, however, because each was determined from a small number of points.

The relationship between chemical shifts in core ionization energies and in proton affinities is not yet fully understood. It is nevertheless clear that from their correlation useful chemical information can be derived that is not readily obtained from either of the two alone.

IX. RELATION OF CORE IONIZATION ENERGIES TO GAS PHASE ACIDITIES

The two processes considered in the preceding chapter, protonation and core ionization of the atom to which the proton attaches, both involve the addition of a positive charge at approximately the same position in the molecule. A general correlation of chemical shifts in their energies was observed. This is a reflection of the fact that differences in either ground-state charge distribution or polarizability that stabilize the protonated ion also tend to stabilize the core-ionized species. A different, but nevertheless interesting, relationship exists between the process of proton removal from a molecule and core ionization of the atom to which the proton is bonded. In this case, inductive effects that stabilize the anion must destabilize the core-ionized species, but increased polarization stabilizes both.

The energy of the proton removal process in the gas phase is a direct measure of the intrinsic acidity of a molecule, unencumbered by solvent effects. As such, it is a quantity of considerable interest, and has been measured for several molecules by observation of proton transfer equilibria with high-pressure mass spectrometry [49-53], or ion cyclotron resonance [54]. This proton removal energy

is called the proton affinity of the anion PA_a, since higher energy means the bound state is favored.

Davis and Shirley [55] have recently employed a proton potential model (PPM) to calculate the proton affinity of several molecules PA and anions PA_a. Their calculation produces individual terms for inductive shifts and relaxation shifts, which are useful in analyzing the intrinsic effects of halogen and alkyl substitution in different series of molecules. Davis and Shirley have also proposed a simple method of obtaining the inductive and relaxation shifts empirically, by using experimental ΔPA and ΔPA_a values for a pair of molecules. This approach has the limitation that the same atom must provide the sites for both the acidic proton and the basic proton, as the oxygen atom does in an alcohol, for example. A more-widely applicable method of empirically separating inductive and relaxation shifts can be developed from the relationship between chemical shifts in anionic proton affinity PA_a and core ionization energy E_i.

In the relaxation potential model (RPM) of Davis and Shirley [56], the core ionization energy shift is given by

$$E_i = -\Delta V(z) - \Delta R_e \qquad \text{(Eq. 9.1)}$$

where $\Delta V(z)$ is the difference in potential energy at the nucleus of the atom to be core-ionized and ΔR_e is the difference in relaxation energy. In the PPM, ΔPA_a is given by

$$\Delta PA_a = -\Delta V_A(1) + \Delta R_a \qquad \text{(Eq. 9.2)}$$

where $\Delta V_A(1)$ is the difference in potential energy at the nucleus of the acid proton and ΔR_a is the corresponding difference in relaxation energy. Since ΔE_i and ΔPA_a are measurable quantities, Eq. 9.1 and 9.2 constitute two equations with four unknowns. Either empirical relationships or plausible assumptions about the relationships between $\Delta V(Z)$ and $\Delta V_A(1)$, and between ΔR_e and ΔR_a, would thus provide enough information to evaluate the four unknown shifts.

Figure 5 is a graph of E_i(O 1s) versus PA_a for eight carboxylic acids. A general correlation is not found, since inductive and relaxation effects oppose each other. In the simplest case, i.e. $\Delta V(Z) = -\Delta V_A(1)$ and $\Delta R_e = -\Delta R_a$,[15] a slope of +1 would be found for relaxation shifts and -1 for inductive shifts. The line in Figure 4 is a linear least-squares fit to the four points CH_3COOH, CFH_2COOH, CF_2HCOOH, and CF_3COOH. Its slope is about -1.1. These four molecules are expected to differ by inductive effects almost exclusively, since fluorine atoms are relatively small and thus difficult to polarize. Thus, on the assumption that ΔR_e and ΔR_a are negligible for these acids, the relationship of

---

[15] $\Delta V(Z)$ and ΔR_e refer to potential energies of an electron, while $\Delta V_A(1)$ and ΔR_a refer to potential energies of a proton, hence the difference in sign.

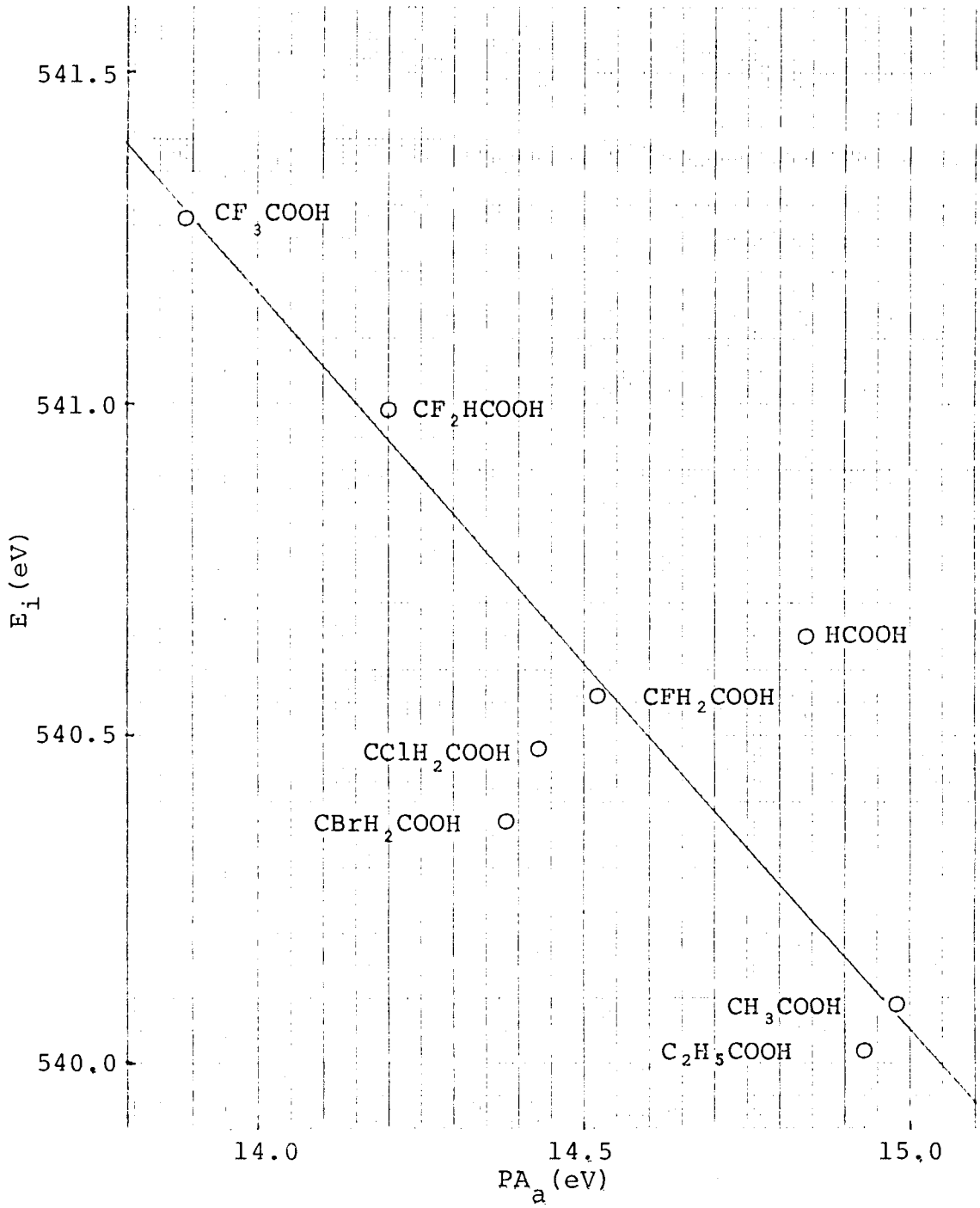

Figure 5. Core ionization energy versus gas phase acidity (anionic proton affinity) for simple and halogen-substituted carboxylic acids.

$\Delta V(Z)$ and $\Delta V_A(1)$ is taken to be

$$\Delta V(Z) = -1.1\ \Delta V_A(1) \qquad \text{(Eq. 9.3)}$$

The only two points in Figure 5 that define a clearly relaxation-dominated shift are C_2H_5COOH and CH_3COOH. Unfortunately, they are too closely spaced to provide a relationship between ΔR_e and ΔR_a. Davis and Shirley [55] argue that $\Delta R_a \approx \Delta R_b$, where ΔR_b is the relaxation shift in the molecular proton affinity. As discussed in the previous chapter, ΔR_e is greater than ΔR_b, but an accurate relationship could not be determined. Assuming, then, that $\Delta R_e > |\Delta R_b| \approx |\Delta R_a|$, the relationship is taken to be

$$\Delta R_e = -1.1\ \Delta R_a \qquad \text{(Eq. 9.4)}$$

The effect of a different choice is discussed below.

It is now possible to solve the above equations for the individual inductive and relaxation shifts. The results for $\Delta V_A(1)$ and ΔR_a are given in Table 3, along with the experimental values of ΔE_i and ΔPA_a, and, for comparison, the values calculated by Davis and Shirley [55] using the proton potential model. In addition to the acids shown in Figure 4, results are given for C_2H_5OH and $(CH_3)_2CHOH$ relative to CH_3OH.

The results from the empirical calculations are in good agreement with those of the semi-empirical PPM calculations. Some interesting trends are evident. The halogens

are about equal in their intrinsic inductive strength, but their polarizability increases markedly with size. The saturation (non-linearity) of the inductive effect is observed in the fluorine-substituted acids. The ΔR_a values for these molecules are not meaningful, however, since the line of zero relaxation shift was fit to these points. The inductive shifts for C_2H_5COOH and for $(CH_3)_2CHOH$ are observed to be negligible compared to the relaxation shifts. This is not shown in the PPM results for the alcohol. Both inductive and relaxation effects are significant in comparing HCOOH and CH_3COOH.

The empirical results listed in Table 3 and discussed above are not extremely sensitive to the numerical relationship assumed for ΔR_e and ΔR_a. If the slope of the general correlation of ΔE_i and ΔPA (-1.6) is assumed to apply to relaxation shifts, then

$$\Delta R_e = -1.6\ \Delta R_b \approx \Delta R_a \qquad \text{(Eq. 9.5)}$$

Employing this relationship instead of Eq. 9.4 introduces a 20 percent reduction in the magnitude of each ΔR_a value and a change of the same magnitude and sign in the corresponding $\Delta V_A(1)$ value. This leaves the trends discussed above essentially unchanged.

While the empirical model relating core ionization energy and gas phase acidity (anionic proton affinity) has

been applied only to hydroxyl (OH) protons, it can in principle be extended to other cases. For example, it would be interesting to consider carbon acids, i.e., compounds in which the most acidic proton is bonded to a carbon atom. Gas phase acidity measurements have been reported for several such compounds [53].

Table 3. Inductive and relaxation shifts in relative gas phase acidities (anionic proton affinities).[a]

Species	Experimental Input		Empirical Results[e]		Theoretical Results[f]	
Acid	ΔPA_a[b]	ΔE_i	$\Delta V_A(1)$	ΔR_a	$\Delta V_A(1)$	ΔR_a
CH_3COOH	(0)	(0)	(0)	(0)	(0)	(0)
CF_3COOH	-25.2	27.4	25.1	-0.1	26.6	1.4
CF_2HCOOH	-18.0	20.7	18.4	0.4	17.0	0.4
CFH_2COOH	-10.8	10.8[c]	10.3	- .5	9.5	0.2
$CClH_2COOH$	-12.8	9.2[c]	10.6	-2.2	9.8	-2.3
$CBrH_2COOH$	-13.9	7.4[c]	10.3	-3.6	-	-
HCOOH	- 3.2	12.9	7.5	4.3	11.2	5.9
C_2H_5COOH	- 2.1	- 2.5[d]	- 0.1	-2.2	- 0.2	-1.8
Alcohol						
CH_3OH	(0)	(0)	(0)	(0)	(0)	(0)
C_2H_5OH	- 1.9	- 7.1	- 2.3	-4.2	- 2.7	-4.9
$(CH_3)_2CHOH$	- 3.1	- 8.8[d]	- 2.4	-5.5	- 5.7	-8.8

[a] All energies are given in kcal/mol.

[b] References [50,51] for acids, reference [54] for alcohols.

[c] Estimated from corresponding ethyl ester shifts for singly-bonded oxygen. See p. 49.

[d] Reference [45].

[e] This work.

[f] Reference [55].

X. EXTENSION OF THE JOLLY AND BAKKE FOUR-PARAMETER EQUATION TO INCLUDE ACIDS AND ESTERS

One approach to the analysis and prediction of substituent effects on chemical reactivity is the four-parameter equation of Swain and Lupton [57]. It is a sum of two terms, one for "field" effects and one for "resonance" effects. Each term consists of a factor related to the sensitivity of the particular type of reaction to that effect and a factor related to the capability of the substituent to generate the effect.

Jolly and Bakke [58] have developed an analogous method of analyzing and predicting substituent effects on the energy of certain gas phase processes that are characterized by the addition of a localized positive charge. These processes include core ionization proton affinity, and lone-pair ionization. Jolly and Bakke determined by least-squares fitting to experimental core ionization energy shifts ΔE_i the parameters necessary for predicting the effects of ten different substituents on 16 classes of molecules. The equation is

$$\Delta E_i = \underline{a}F + \underline{b}R \qquad \text{(Eq. 10.1)}$$

where F and R represent the σ and π electronegativity of the substituent, respectively, and $\underline{a}$ and $\underline{b}$ represent the sensitivity of the particular core ionization energy in the

particular class of molecules to these effects. Jolly and Bakke [58] reported 92 predicted and experimental ΔE_i values with an average deviation between the two of ±.20 eV.

Jolly and Bakke included carbon 1s and oxygen 1s shifts in six symmetric carbonyl compounds OCX_2.[16] Most of the molecules included in the present study are asymmetric carbonyls $OC\langle^{X}_{Y}$. It is proposed that the four-parameter equation can be extended to these by the simple method of averaging the F and R values for two substituents.

$$\Delta E_i = \underline{a}\left(\frac{Fx+Fy}{2}\right) + \underline{b}\left(\frac{Rx+Ry}{2}\right) \qquad \text{(Eq. 10.2)}$$

The calculated ionization energies for the first three compounds in Table 4 were computed using Eq. 10.2 and the appropriate values of $\underline{a}$, $\underline{b}$, F, and R given by Jolly and Bakke [58]. The average deviation from experiment is 0.1 eV (C 1s) and 0.2 eV (O 1s). The averaging of F and R values appears to match experimental results as accurately as the original method does. This finding suggests that many more compounds could be included in the least-squares fits, enabling a more definitive determination of some F and R values, as well as extension of the method to other substituents and molecular types.

---

[16] The carbon 1s parameters are somewhat suspect because the reference level used by Jolly and Bakke -- E_i(H CO, C 1s) = 294.21 eV -- differs substantially from the recently reported value of 294.47 eV [46].

The data for carbonyl carbon 1s and oxygen 1s shifts from this study have been employed to determine approximate F and R values for two additional substituents, -OH and $-OC_2H_5$. For the hydroxyl group, both F and R are intermediate between the corresponding substituent constants for fluorine and chlorine (given by Jolly and Bakke). For the ethoxy group, both constants are slightly greater in magnitude than those for the methoxy group. The constants a and b have been evaluated approximately for one additional molecular type, $CXH_2COOC_2H_5$. Sixteen shifts have been predicted and have an average deviation from experiment of 0.1 eV (C 1s) and 0.2 eV (O 1s). The predicted and experimental ionization energies are given in Table 4 and the newly determined constants in Table 5.

Table 4. Experimental and empirically-calculated carbonyl core ionization energies (eV).

Compound	Carbon 1s		Oxygen 1s	
	E_i(expt)	E_i(calc)	E_i(expt)	E_i(calc)
$HCOOCH_3$	295.14	295.02	538.45	538.68
CH_3COOCH_3	294.85	294.80	537.92	537.69
CF_3COOCH_3	295.93	295.80	539.03	539.18
CH_3COOH	295.38	295.58	538.29	538.04
CF_3COOH	296.55	296.57	539.56	539.52
$CH_3COOC_2H_5$	294.76	294.77	537.78	537.30
$CF_3COOC_2H_5$	295.72	295.76	538.83	538.78
$CClH_2COOC_2H_5$	295.01	295.84	538.10	537.92

Table 5. Additional constants for the Jolly and Bakke equation.

Substituent	F	R	Experimental Energies Used
-OH	1.24	-11.2	HCOOH (C 1s, O 1s)
$-OC_2H_5$	.764	- 8.76	$HCOOC_2H_5$ (C 1s, O 1s)
Class of Molecule	**a**	**b**	**Experimental Energies Used**
$CXH_2CO^*OC_2H_5$	2.52	.296	$CH_3COOC_2H_5$ (O 1s)
			$CFH_2COOC_2H_5$ (O 1s)
			$CBrH_2COOC_2H_5$ (O 1s)
$CXH_2C^*OOC_2H_5$	2.58	.312	$CH_3COOC_2H_5$ (C 1s)
			$CFH_2COOC_2H_5$ (C 1s)
			$CBrH_2COOC_2H_5$ (C 1s)

BIBLIOGRAPHY

1. K. Siegbahn and K. Edvarson, Nucl. Phys. 1, 137 (1956).

2. K. Siegbahn, C. Nordling, A. Fahlman, R. Nordberg, K. Hamrin, J. Hedman, G. Johansson, T. Bergmark, S. E. Karlsson, J. Lindgren, and B. Lindberg, ESCA -- Atomic, Molecular and Solid State Structure Studied by Means of Electron Spectroscopy, Almqvist and Wiksells, Uppsala, 1967.

3. J. M. Hollander, in Electron Spectroscopy, D. A. Shirley (Ed.), North-Holland Publishing Company, Amsterdam, 1972, p. 9.

4. T. A. Carlson, J. Electron Spectrosc. Relat. Phenom., 5, xvii (1974).

5. T. A. Carlson, Photoelectron and Auger Spectroscopy, Plenum Press, New York, 1975, pp. 1-12.

6. R. W. Shaw, Jr., T. X. Carroll, and T. D. Thomas, J. Amer. Chem. Soc., 95, 5870 (1973).

7. R. W. Shaw, Jr., and T. D. Thomas, Chem. Phys. Lett., 22, 127 (1973).

8. T. X. Carroll and T. D. Thomas, J. Chem. Phys., 60, 2186 (1974).

9. T. X. Carroll, R. W. Shaw, Jr., T. D. Thomas, C. Kindle, and N. Bartlett, J. Amer. Chem. Soc., 96, 1989 (1974).

10. J. S. Jen and T. D. Thomas, J. Electron Spectrosc. Relat. Phenom., 4, 43 (1974).

11. J. S. Jen and T. D. Thomas, J. Amer. Chem. Soc., 97, 1265 (1975).

12. P. H. Citrin, R. W. Shaw, Jr., and T. D. Thomas, in Electron Spectroscopy, D. A. Shirley (Ed.), North-Holland Publishing Company, Amsterdam, 1972, p. 105.

13. K. Läuger, J. Phys. Chem. Solids, 32, 609 (1971).

14. T. D. Thomas and R. W. Shaw, Jr., J. Electron Spectrosc. Relat. Phenom., 5, 1081 (1974).

15. J. A. Bearden, Rev. Mod. Phys., 39, 78 (1967).

16. B. N. Taylor, W. H. Parker, and D. N. Langenberg, ibid., 41, 375 (1969).

17. J. E. Castle, L. B. Hazell, and R. D. Whitehead, J. Electron Spectrosc. Relat. Phenom., 9, 247 (1976).

18. M. Green and V. E. Cosslett, Brit. J. Appl. Phys. (J. Phys. D), 1, 425 (1968).

19. N. A. Dyson, X-rays in Atomic and Nuclear Physics, Longman Group Ltd., London, 1973, p. 138.

20. Reference 12, p. 112.

21. Reference 5, p. 20.

22. F. Kreith, Principles of Heat Transfer, International Textbook Company, Scranton, 1958, p. 18.

23. Ibid., pp. 187, 192.

24. R. J. Corruccini, Vacuum, 7-8, 19 (1959).

25. Reference 22, p. 11.

26. E. J. McGuire, Phys. Rev., 175, 20 (1968).

27. B. L. Henke, Technical Report, AFOSR 72-1140, April 1972.

28. C. Nordling, E. Solokowski, and K. Siegbahn, Arkiv Fysik, 13, 483 (1958).

29. D. W. Davis, D. A. Shirley, and T. D. Thomas, J. Amer. Chem. Soc., 94, 6565 (1972).

30. Reference 4, p. xviii.

31. D. A. Shirley, J. Electron Spectrosc. Relat. Phenom., 5, 146-7 (1974).

32. K. Kimura, T. Yamazaki, and K. Osafune, J. Electron Spectrosc. Relat. Phenom., 6, 391 (1975).

33. J. C. Boyce, Phys. Rev., 46, 378 (1934).

34. P. R. Bevington, Data Reduction and Error Analysis for the Physical Sciences, McGraw-Hill, New York, 1969, p. 60.

35. S. R. Smith and T. D. Thomas, J. Electron Spectrosc. Relat. Phenom., 8, 45 (1976).

36. H. Schrenk and P. S. Bagus, unpublished results quoted in reference [37].

37. J. Cambray, J. Gasteiger, A. Streitwieser, Jr., and P. S. Bagus, J. Amer. Chem. Soc., 96, 5978 (1974).

38. R. L. Martin and D. A. Shirley, J. Amer. Chem. Soc., 96, 5299 (1974).

39. Ibid., p. 5302, Table II.

40. D. W. Davis, and J. W. Rabalais, J. Amer. Chem. Soc., 96, 5305 (1974).

41. T. X. Carroll, S. R. Smith and T. D. Thomas. J. Amer. Chem. Soc., 97, 659 (1975).

42. Reference [40], p. 5309.

43. C. V. Pesheck and S. E. Buttrill, Jr., J. Amer. Chem. Soc., 96, 6027 (1974).

44. J. F. Wolf, R. H. Staley, I. Koppel, M. Taagepera, R. T. McIver, Jr., J. L. Beauchamp, and R. W. Taft, submitted for publication.

45. B. E. Mills, R. L. Martin and D. A. Shirley, J. Amer. Chem. Soc., 98, 2380 (1976).

46. T. X. Carroll and T. D. Thomas, J. Electron Spectrosc. Relat. Phenom., in press.

47. Y. K. Lau and P. Kebarle, J. Amer. Soc., 98, 7452 (1976).

48. R. Yamdagni and P. Kebarle, J. Amer. Chem. Soc., 98, 1320 (1976).

49. R. Yamdagni and P. Kebarle, ibid., 93, 7139 (1971).

50. R. Yamdagni and P. Kebarle, ibid., 95, 4050 (1973).

51. K. Hiraoko, R. Yamdagni, and P. Kebarle, ibid., 95, 6833 (1973).

52. T. B. McMahon and P. Kebarle, ibid., 96, 5940 (1974).

53. T. B. McMahon and P. Kebarle, ibid., 98, 3399 (1976).

54. R. T. McIver, J. A. Scott, and J. H. Silvers, "Twenty-First Annual Conference on Mass Spectrometry and Allied Topics," San Francisco, California, May, 1973, Abstract A2 (see J. Chem. Soc., Chem. Comm. 1974, 10, 403).

55. D. W. Davis and D. A. Shirley, J. Amer. Chem. Soc., in press.

56. D. W. Davis and D. A. Shirley, J. Electron Spectrosc. Relat. Phenom., 3, 137 (1974).

57. C. G. Swain and E. C. Lupton, J. Amer. Chem. Soc., 90, 4328 (1968).

58. W. L. Jolly and A. A. Bakke, ibid., 98, 6500 (1976).

59. Reference 34, p. 73.

APPENDICES

APPENDIX A

COMPUTATION OF EXPERIMENTAL AND MEAN-VALUE UNCERTAINTIES

The uncertainty in the focusing voltage corresponding to each particular calibrant or sample peak was computed by applying the formula [34]

$$\sigma_x^2 = \Sigma_v [\partial x/\partial v)^2 \sigma_v^2] \qquad \text{(Eq. 6.2)}$$

including contributions from the actual voltage measurement (itself a function of voltage), the peak position given by least-squares fitting, and the average channel width. The focusing voltages pertaining to each individual ionization energy measurement were combined into a ratio, called rho, which thus contained all the experimental information for that measurement. For neon 1s-2s calibration, rho was defined as [V(sample) - V(Ne 1s)]/[V(Ne 2s) - V(Ne 1s)]. For internal calibration, rho was simply V(sample)/V(calibrant). The experimental component of the uncertainty in each ionization energy measurement was thus given by

$$\sigma_{expt}^2 = (\partial E/\partial \rho)^2 \sigma_\rho^2 \qquad \text{(Eq. A.1)}$$

where E represents the expression for the ionization energy as a function of rho that is appropriate to the particular calibration method.

The uncertainties σ_{E_j} thus determined for each measured ionization energy E_j were used in the calculation of weighted-mean values $\bar{E}$ according to the formula [59]

$$\bar{E} = \sum_{j=1}^{n} (E_j W_j) \qquad \text{(Eq. A.2)}$$

where

$$W_j \equiv (1/\sigma_{E_j}^2) / \sum_{j=1}^{n} (1/\sigma_{E_j}^2) \qquad \text{(Eq. A.3)}$$

and n is the number of individual measurements.

If all of the E_j values contributing to a particular $\bar{E}$ were calibrated in the same way, the individual calibration uncertainties $\sigma_{E_{jcal}}$ would be approximately equal; and, any error due to the calibration constants would have essentially the same effect on all the E_j values and thus on $\bar{E}$. However, the individual experimental uncertainties $\sigma_{E_{jexpt}}$ can be handled as uncorrelated errors. Thus the uncertainty of the mean for similarly-calibrated measurements $\sigma_{\bar{E}}$ was computed as follows

$$\sigma_{\bar{E}}^2 = (\bar{\sigma}_{E_{jcal}})^2 + \sum_{j=1}^{n} [(\sigma_{E_{jexpt}})^2 W_j^2] \qquad \text{(Eq. A.4)}$$

In the case that all the $\sigma_{E_{jcal}}$ values are equal and all the $\sigma_{E_{jexpt}}$ values are equal, this reduces to

$$\sigma_{\bar{E}}^2 = (\sigma_{E_{jcal}})^2 + \frac{1}{n}(\sigma_{E_{jexpt}})^2. \qquad \text{(Eq. A.5)}$$

In cases involving more than one method of calibration, $\bar{E}$ was computed for each method, and the weighted mean of those values was reported. Its uncertainty was computed as above, assuming the experimental uncertainties to be uncorrelated and the calibration uncertainties to be correlated or uncorrelated, depending on the individual case.

APPENDIX B

CORE IONIZATION POTENTIALS IN CARBON MONOXIDE

Journal of Electron Spectroscopy and Related Phenomena, 8 (1976) 45–49

CORE IONIZATION POTENTIALS IN CARBON MONOXIDE

STEVEN R. SMITH AND T. DARRAH THOMAS

Department of Chemistry and Radiation Center, Oregon State University, Corvallis, Oregon 97331 (U.S.A.)

(Received 24 June 1975)

ABSTRACT

Conflicting values have been reported for the core ionization potentials in carbon monoxide. We have remeasured these and find 296.24 ± 0.03 for the carbon 1s ionization potential and 542.57 ± 0.03 for oxygen 1s. The carbon value is close to previously reported values; that for oxygen is higher by ~ 0.5 eV. These results are compared with ionization potentials calculated from molecular orbital theory. The value predicted by near-Hartree–Fock calculations for oxygen is too low by ~ 1eV and that for carbon is too high by ~ 0.5 eV.

INTRODUCTION

Carbon monoxide is a small molecule that plays an important role in molecular structure theory. Because of its simple geometry and small number of electrons, it is susceptible to theoretical investigation by the most sophisticated techniques. At the same time, it has been found that the properties of carbon monoxide are not accurately predicted unless proper consideration is given to correlation effects. For instance, the Hartree–Fock molecular orbital theory fails to predict the sign of the dipole moment; the importance of including configuration interaction in order to account for the dipole moment has been reviewed by Schaefer[1]. The comparison between experimental measurements and theoretically calculated quantities, therefore, provides a useful test of the extent to which a theoretical calculation has adequately included correlation effects.

Hole-state Hartree–Fock calculations for carbon monoxide missing a core electron from either atom compared with Hartree–Fock calculations for the neutral molecule give theoretical predictions of the core ionization potentials[2, 3]. For the oxygen 1s electron the theoretical values differ from the experimental values by between zero and 0.5 eV; the different experimental values, however, disagree from one another also by ~ 0.5 eV[4–7]. It is clear that a more accurate measurement is

needed. For the carbon 1s electrons the disagreement between theory and experiment is over 2 eV; the disagreement among experimental values is, however, only ~ 0.4 eV.

From the point of view of the experimental photoelectron spectroscopist, accurate knowledge of the core ionization potentials of carbon monoxide is important. The oxygen 1s ionization potential (542.6 eV) is well separated from the ionization potentials of oxygen in various organic compounds (538–541 eV). It provides, therefore, a convenient internal standard against which to measure these energies. No other simple compound is so convenient; NO and O_2 have multiplet lines; CO_2 and N_2O have ionization potentials that overlap the range of typical ionization potentials in organic compounds.

The published values of the core ionization potentials in carbon monoxide are in substantial disagreement with one another. For oxygen 1s, values of 542.1 eV[4], 542.3 eV[5], 542.6 eV[6] have been reported. From the CO–CO_2 shift given by Davis et al. (1.5 eV[7]) and the accurately known ionization potential for CO_2 (541.3 eV[8]) we calculate 542.8 eV. From the CO–CO_2 shift given by Siegbahn et al. (1.3 eV[9]) we have 542.6 eV. The uncertainty in this quantity is an order of magnitude greater than one would expect from the current state of the art. For the carbon 1s electrons the values from the same sources are 295.9 eV, 296.2 eV, 296.2 eV, 296.3 eV, and 296.1 eV. The uncertainty is smaller for carbon than for oxygen, but still well beyond what is easily possible. We report here the accurate measurement of these ionization potentials.

EXPERIMENTAL PROCEDURE

All measurements were made in the gas phase, using our cylindrical mirror analyzer[10]. Total gas pressure in the sample cell was ~ 0.1 torr. The exciting radiation was either MgKα (1253.619 $\pm$ 0.026 eV[11, 12]) or AlKα (1486.582 $\pm$ 0.019 eV[8]).

Two methods were used to determine the core ionization potentials of interest. In the first, the photoelectron spectra of a mixture of CO and CO_2 were run and the differences between the two carbon 1s and between the two oxygen 1s ionization potentials were determined. The absolute values of the ionization potentials, for CO_2 are accurately known (oxygen: 541.32 $\pm$ 0.05 eV[8], 541.28 $\pm$ 0.12 eV[13]; carbon 297.71 $\pm$ 0.05 eV[8], 297.69 $\pm$ 0.14 eV[13]); we have used the values reported by Thomas and Shaw[8], which have the smaller uncertainty.

In the second method, carbon monoxide and neon were run simultaneously. Successive scans were made of the neon 1s, neon Auger or neon 2s, oxygen 1s, and carbon 1s spectra. The neon energies are known with an accuracy of better than 0.02 eV[8], and provide convenient calibration standards for the spectrometer.

Peak positions were determined by least-squares fits of Voigt functions to the data. Focussing voltages were measured with a Julie TD-1000 Differential Voltmeter. Corrections were made, where needed, for relativistic effects in the spectrometer (about 0.02 eV[8]) and for recoil of the final ion (about 0.02 eV). The results of our

TABLE 1

CORE IONIZATION POTENTIALS FOR CO (eV)

	CO_2 calibration	*Ne calibration*	*Average*
C(1s)	296.25	296.24	296.24
O(1s)	542.59	542.56	542.57

measurements are summarized in Table 1. Including all sources of error, we estimate that the average values have an uncertainty of $\sim$ 0.03 eV.

DISCUSSION

Experimental values

The carbon 1s ionization potential of 296.24 eV is in reasonable accord with the previously reported values, most of which are either 296.2 or 296.3 eV. The oxygen 1s ionization potential of 542.57 eV, however, differs rather markedly from the earlier values given by Siegbahn et al.[4] and by Thomas[5]. There are similar discrepancies between the fluorine 1s ionization potentials originally reported by these workers and their more recent values. The early measurements by Thomas[5, 14, 15] were based on calibration using neon valence-shell ionization potentials and ignoring any possible voltage offset between the sample cell and the rest of the spectrometer. This procedure can lead to a systematic error that is greatest for low kinetic energies (high ionization potentials).

Exactly such a trend is seen in a comparison of the early work and more recent work reported by Thomas and co-workers. For neon 1s the difference between the early[14] and most recent[8] value is 0.6 eV; for fluorine 1s[15] the difference is 0.5 eV; oxygen 1s[5], 0.3 eV; carbon 1s[5], no difference.

TABLE 2

COMPARISON BETWEEN EXPERIMENT AND THEORETICAL IONIZATION POTENTIALS FOR CORE ELECTRONS OF CO (Energies in eV)

	Expt.	*Theory*			
		a	*b*	*c*	*d*
C(1s)	296.24	298.37	305.3	298.20	296.87
O(1s)	542.57	542.09	551.0	542.55	541.57

a, Reference 16; b, reference 17; c, reference 2; d, reference 3.

Comparison with theoretical values

Several theoretical values for the core ionization potentials of carbon monoxide have been calculated. These are presented, together with the experimental values, in Table 2. Column a gives the theoretical results obtained by Hillier et al.[16] who have used a configuration–interaction calculation to estimate the relaxation energy in the final ion together with the orbital energies of a Hartree–Fock calculation to give the ionization potentials. Their value for oxygen 1s is reasonably close (0.5 eV) to the experimental value; that for carbon 1s is, however, off by 2 eV.

In column b are listed values of the ionization potentials calculated by Connolly et al.[17] using the multiple-scattering Xα method. This procedure gives results that are in better agreement with experiment than are the orbital energies of a Hartree–Fock calculation; it is computationally simpler. As seen here, however, and as noted by Connolly et al., it fails to predict core ionization potentials by as much as 9 eV.

Columns c and d give values calculated from the difference between Hartree–Fock energies of the neutral molecule and final ion with the appropriate hole state. The values in column c have been reported by Cambray et al.[2] and are based on a double-zeta basis set augmented with 3d functions. The agreement between experiment and theory for the oxygen 1s value is astonishingly, but fortuitously, good. When a larger basis set is chosen the agreement is not as good (see below). The theoretical carbon 1s value is too high by $\sim$ 2 eV.

The results given in column d have been obtained by Schrenk and Bagus[3] using a large basis set (7s6p3d2f) and are thought to be close to the Hartree–Fock values[18]. The remaining discrepancies between experiment and theory are presumably due to correlation and relativistic effects. The predicted value for oxygen is $\sim$ 1 eV too low, while that for carbon is $\sim$ 0.5 eV too high; the remaining corrections are in opposite directions. The magnitude of these discrepancies is about what one would expect for the correlation energy correction.

As a result of a multiconfiguration self-consistent-field calculation of the dipole moment of CO, Billingsley and Krauss[19] have concluded that important configurations (beyond the Hartree–Fock configuration) for the ground state of CO are those that involve transfer of π electrons from the oxygen to the carbon. If the same sort of configurations are important for the core-ionized species, then the relative signs of the correlation energies to the core ionization potentials are readily explained by the following argument. We first note that the calculated ionization potential (which contains no correlation-energy correction) will be greater than the measured value if the correlation for the ion is greater than that for the neutral molecule and less if the reverse is true. For carbon monoxide the transfer of an electron from oxygen to carbon will be favored in the species $C^{*+}O$ and disfavored in the species CO^{*+} relative to the neutral species CO. We, therefore, expect larger correlation energy for $C^{*+}O$ than for CO and smaller correlation energy for CO^{*+} than for CO, as is observed.

ACKNOWLEDGMENT

This work was supported in part by the United States Energy Research and Development Administration.

REFERENCES

1 H. F. Schaefer, *The Electronic Structure of Atoms and Molecules*, Addison, Wesley Publishing Co., 1972, p. 196.
2 J. Cambray, J. Gasteiger, A. Streitwieser, Jr. and P. S. Bagus, *J. Amer. Chem. Soc.*, 96 (1974) 5978.
3 H. Schrenk and P. S. Bagus, unpublished results quoted in ref. 2.
4 K. Siegbahn, et al., *ESCA Applied to Free Molecules*, North-Holland Publishing Co., Amsterdam, 1969, p. 76.
5 T. D. Thomas, *J. Chem. Phys.*, 53, 1744 (1970).
6 R. W. Shaw, Jr. and T. D. Thomas, *Chem. Phys. Lett*, 14 (1972) 121.
7 D. W. Davis, J. M. Hollander, D. A. Shirley and T. D. Thomas, *J. Chem. Phys.*, 52 (1970) 3295.
8 T. D. Thomas and R. W. Shaw, Jr., *J. Electron Spectrosc.*, 5 (1974) 1081.
9 Ref. 4, p. 126.
10 P. H. Citrin, R. W. Shaw, Jr. and T. D. Thomas, in D. A. Shirley (Ed.), *Electron Spectroscopy*, North-Holland Publishing Co., Amsterdam, 1972, p. 105.
11 J. A. Bearden, *Rev. Mod. Phys.*, 39 (1967) 78. The value given by Bearden in A* units has been converted to eV using the constants given in ref. 12.
12 B. N. Taylor, W. H. Parker and D. N. Langenberg, *Rev. Mod. Phys.*, 41 (1969) 375.
13 G. Johansson, J. Hedman, A. Berndtsson, M. Klasson and R. Nilsson, *J. Electron Spectrosc.*, 2 (1973) 295.
14 T. D. Thomas, *J. Chem. Phys.*, 52 (1970) 1373.
15 T. D. Thomas, *J. Amer. Chem. Soc.*, 92 (1970) 4184.
16 I. H. Hillier, V. R. Saunders and M. H. Wood, *Chem. Phys. Lett.*, 7 (1970) 323.
17 J. W. D. Connolly, H. Siegbahn, U. Gelius and C. Nordling, *J. Chem. Phys.*, 58 (1973) 4265.
18 P. S. Bagus, private communication.
19 F. P. Billingsley and M. Krauss, *J. Chem. Phys.*, 60 (1974) 4130.

APPENDIX C

CORRELATION BETWEEN PROTON AFFINITY AND CORE-ELECTRON IONIZATION POTENTIALS FOR DOUBLE-BONDED OXYGEN. SITE OF PROTONATION IN ESTERS

[Reprinted from the Journal of the American Chemical Society, 97, 659 (1975).]

Correlation between Proton Affinity and Core-Electron Ionization Potentials for Double-Bonded Oxygen. Site of Protonation in Esters

Sir:

A striking correlation of the proton affinities of a number of alcohols and amines with the core-electron ionization potentials of oxygen or nitrogen in the same molecule has been pointed out by Martin and Shirley[1] and by Davis and Rabalais.[2] The change in proton affinity from one molecule to another is almost exactly equal to the change in core ionization potential. The reason for this result is that the removal of a core electron from the oxygen or nitrogen is electrically equivalent to the addition of a proton at the same site. It was suggested by Martin and Shirley that the ionization-potential shifts and proton affinities might be comparable over a wider range than they had considered.

Davis and Rabalais found, however, that the point for acetone fell off of their correlation line by about 1 eV and that the point for formic acid was off by nearly 0.5 eV. They concluded, therefore, that double-bonded oxygen does not fit the correlation and proposed a number of reasons to account for the phenomenon.

We have recently remeasured the oxygen 1s ionization potential in acetone to be 537.92 eV, in substantial disagreement with the previously reported value of 539.0 eV.[3] Our new value falls quite close to the correlation line for the alcohols. In addition, we have measured oxygen 1s ionization potentials for methyl acetate (537.87 and 539.43 eV), formaldehyde (539.42 eV[4]), and acetaldehyde (538.62 eV[5]) and have remeasured this quantity for formic acid (538.92 and 540.60 eV[6]). These ionization potentials also fall quite close to the same correlation line.[7]

We have extended this comparison of proton affinities and inner-shell ionization potentials by considering O_2, NO, CO_2, CO, and N_2O—rather different molecules from those previously considered—together with a recent measurement we have made on methyl ether.[8]

The correlation of proton affinity with core ionization potential is shown in Figure 1. The data previously presented by Martin and Shirley and by Davis and Rabalais are shown as open circles, the additional results[9] mentioned above as filled circles. The line is a least-squares fit, constrained to a slope of -1, to all of the data except those for CO, NO, N_2O, and O_2, and corresponds to the relationship IP(1s) + PA = 546.84 eV. We see that, except for the diatomic molecules, all of the points fall within about 0.2 eV of the line, in agreement with the suggestion made by Martin and Shirley that this relationship should hold for a wide class of compounds. Even the diatomic molecules, although falling farther off the line, are in agreement with the general trend.

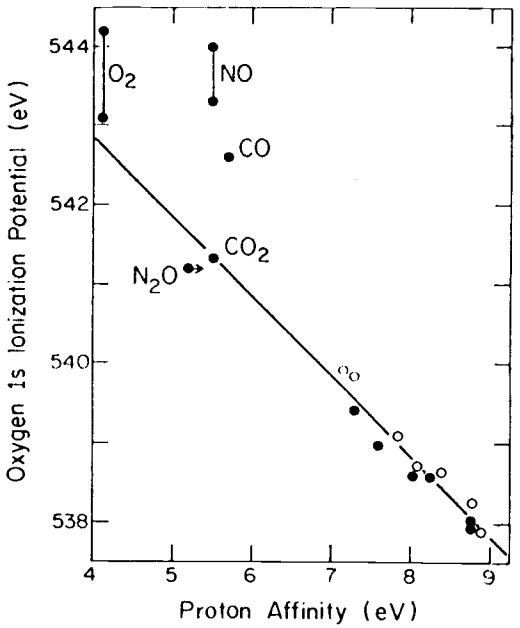

Figure 1. Correlation of oxygen 1s ionization potentials with proton affinities. Open circles represent data previously discussed in ref 1 and 2. Filled circles represent new results. The unlabeled solid circles in the lower right represent, from top to bottom, H_2CO, HCOOH, CH_3CHO, $(CH_3)_2O$, CH_3COOCH_3, and $(CH_3)_2CO$. The open circles represent, from top to bottom, H_2O, CF_3CH_2OH, CH_3OH, CH_3CH_2OH, $(CH_3)_2CHOH$, $(CH_3)_3COH$, and $(C_2H_5)_2O$. For carboxyl oxygens only the lower of the two ionization potentials has been used. The proton affinity for N_2O has been reported only as a lower limit.

A closer inspection of the data shows that the points for the double-bonded oxygen fall consistently lower than those for single-bonded oxygen. If these data are fit separately with lines of slope = −1, these are displaced from one another by 0.25 eV. The root-mean-square deviation of the points from their respective lines is about 0.1 eV, which is comparable to the experimental error in the measurement of both proton affinity and core ionization potential. This slight difference between the two kinds of oxygen may, as has been pointed out by Davis and Rabalais, arise from the different hybridization involved in single and double bonds.

For formic acid and methyl acetate there are two oxygen 1s ionization potentials, one for the keto oxygen and one for the ether oxygen. The lower of these correlates well with the proton affinity; the higher falls about 1.5 eV above the line. Protonation evidently occurs at the oxygen with the lower 1s ionization potential. Inspection of the other data reveals that keto oxygens have lower core ionization potentials than do ether oxygens in similar compounds. The molecular orbital calculations of Snyder and Basch[10] predict that the keto oxygen in formic acid will have the lower ionization potential. Combining these observations we conclude that protonation occurs at the keto oxygen. This conclusion is the reverse of that reached by Pesheck and Buttrill[11] from ion-cyclotron-resonance results.

We have mentioned above new results and remeasured results for oxygen 1s ionization potentials. These were measured on mixtures of the gas of interest with either carbon dioxide or carbon monoxide as a reference compound so that any drifts in the spectrometer focusing voltage were compensated. The oxygen 1s ionization potential in carbon dioxide is accurately known, having been measured independently in separate laboratories to be 541.32 ± 0.05[12] and 541.28 ± 0.12 eV.[13] We have recently remeasured the oxygen 1s ionization potential in carbon monoxide to be 542.58 eV,[14] somewhat higher than previously reported values.[3,15]

Acknowledgment. This work was supported in part by the U.S. Atomic Energy Commission.

References and Notes

(1) R. L. Martin and D. A. Shirley, *J. Amer. Chem. Soc.*, **96,** 5299 (1974).
(2) D. W. Davis and J. W. Rabalais, *J. Amer. Chem. Soc.*, **96,** 5305 (1974).
(3) K. Siegbahn, C. Nordling, G. Johansson, J. Hedman, P. F. Heden, K. Hamrin, U. Gelius, T. Bergmark, L. O. Werme, R. Manne, and Y. Baer, "ESCA Applied to Free Molecules," North-Holland Publishing Co., Amsterdam, 1969, p 126.
(4) T. X. Carroll and T. D. Thomas, *J. Electron Spectrosc. Relat. Phenom.*, to be submitted for publication.
(5) This result is in substantial disagreement with the previously reported value of 537.6 eV, ref 3.
(6) These results are in accord with the formic acid–carbon dioxide differences reported by D. W. Davis, J. M. Hollander, D. A. Shirley, and T. D. Thomas, *J. Chem. Phys.*, **52,** 3295 (1970). The actual values are, however, higher, and the value for the double bonded oxygen is closer to the correlation line than that plotted by Davis and Rabalais.
(7) Proton affinities have been taken from J. Long and B. Munson, *J. Amer. Chem. Soc.*, **95,** 2427 (1973); A. E. Roche, M. M. Sutton, D. K. Bohme, and H. I. Schiff, *J. Chem. Phys.*, **55,** 5480 (1971).
(8) S. Jen and T. D. Thomas, *J. Electron Spectrosc. Relat. Phenom.*, **4,** 43 (1974).
(9) Ionization potentials are from ref 3, 8, 12, 13, and 14. Proton affinities are from ref 7.
(10) L. C. Snyder and H. Basch, "Molecular Wave Functions and Properties," Wiley, New York, N.Y., 1972.
(11) C. V. Pesheck and S. E. Buttrill, *J. Amer. Chem. Soc.*, **96,** 6027 (1974). NOTE ADDED IN PROOF: We have recently measured the oxygen 1s spectrum for dimethyl carbonate, which has two ether oxygens and one keto oxygen. In the photoelectron spectrum, the peak with relative intensity 2 (ether) corresponds to the higher ionization potential, substantiating our conclusions.
(12) R. W. Shaw, Jr., and T. D. Thomas, *J. Electron Spectrosc. Relat. Phenom.*, **5,** 1081 (1974).
(13) G. Johansson, J. Hedman, A. Berndtsson, M. Klasson, and R. Nilsson, *J. Electron Spectrosc. Relat. Phenom.*, **2,** 295 (1973).
(14) S. R. Smith and T. D. Thomas, to be submitted for publication.
(15) T. D. Thomas, *J. Chem. Phys.*, **53,** 1744 (1970).

T. X. Carroll, S. R. Smith, T. D. Thomas*
Department of Chemistry and Radiation Center
Oregon State University
Corvallis, Oregon 97331
Received October 29, 1974

APPENDIX D

COMPLETE TABULATION OF CORE IONIZATION ENERGIES FROM THIS STUDY[a]

Compound	(subst) -CH_3	$\overset{O}{\overset{\|}{C}}$	CH_2 or -CH_3	-CH_3	$-O-$	=O
HCOOH		295.80(6)			540.65(3)	539.00(3)
CH_3COOH	291.55(4)	295.38(4)			540.09(3)	538.29(3)
CF_3COOH	299.28(4)	296.55(4)			541.28(3)	539.56(3)
CF_2HCOOH	296.39(4)[c]	296.39(4)[c]			540.99(3)	539.25(3)
CFH_2COOH[b]					540.56	538.76
$CClH_2COOH$[b]					540.48	538.68
$CBrH_2COOH$[b]					540.37	538.57
$HCOOCH_3$		295.14(3)	292.78(3)		539.88(3)	538.45(3)
CH_3COOCH_3	291.30(5)	294.85(5)	292.55(5)		539.46(3)	537.92(3)
CF_3COOCH_3	299.03(5)	295.93(5)	293.34(5)		540.48(3)	539.03(3)
$HCOOC_2H_5$		294.99(7)	292.57(7)	291.04(8)	539.58(3)	538.26(3)
$CH_3COOC_2H_5$	291.07(4)[c]	294.76(4)	292.45(4)	291.07(4)[c]	539.20(3)	537.78(3)
$CF_3COOC_2H_5$	298.86(3)	295.72(3)	293.07(3)	291.37(3)	540.15(4)	538.83(4)
$CF_2HCOOC_2H_5$	295.79(5)[c]	295.79(5)[c]	292.85(6)	291.18(6)	539.91(3)	538.57(3)
$CFH_2COOC_2H_5$	293.70(5)	295.05(4)	292.58(5)	291.06(5)	539.57(3)	538.17(3)
$CClH_2COOC_2H_5$	292.64(3)[c]	295.01(4)	292.64(3)[c]	291.07(4)	539.52(3)	538.10(3)
$CBrH_2COOC_2H_5$	292.38(4)[c]	294.96(4)	292.38(4)[c]	290.90(4)	539.45(3)	538.01(3)
$CH_3OCOOCH_3$		296.14(4)	292.75(4)		539.75(3)	538.06(3)
CH_3COCH_3		293.71(4)	291.15(3)			537.96(3)
CO		C 1s: 296.24(3)		O 1s: 542.57(3)		

[a] All energies are given in eV, with the uncertainty of the last digit in parentheses.

[b] The E_i(O 1s) values were estimated from the corresponding ethyl ester values. See p. 49.

[c] The average ionization energy for two inequivalent carbons is given; the peaks were unresolvable.